Prof. Masayuki Ishihara (National Defense Medical College, Tokorozawa, Japan) [26, 27]. HS preparations from bovine intestine, aorta, and lung were kindly provided by Keiichi Yoshida (Seikagaku Corp., Tokyo, Japan) [28]. HS and CS/DS from bovine liver were prepared as described previously [29]. Recombinant heparinases I and III from *Flavobacterium heparinum* were from IBEX Technologies, Montreal, Canada. Anti-myc antibody, anti-V5 antibody, and ECL anti-mouse IgG horseradish peroxidase-linked whole antibody (from sheep) were obtained from Invitrogen Co., Carlsbad, CA. Phosphatase-labeled anti-mouse IgG+IgM (H+L) antibody was from Kirkegaard & Perry Laboratories, Inc., Geithersburg, MA. A soluble form of the recombinant envelope glycoprotein E1 of genotype 1b (comprising amino acids 192–340) with a V5 and His6 tag fusion protein or E2 of genotype 1b (comprising amino acids 384–711) with a myc and His6 tag fusion protein was generated using a baculovirus/HighFive cell system at 27 °C with Sf-900 II SFM insect cell medium (GIBCO) containing 10 % (v/v) fetal bovine serum (FBS). The expressed proteins were purified using a QIAexpress Protein Purification System (QIAGEN), following a protocol provided by the manufacturer. Concentration of the purified E1 and E2 proteins was estimated on the basis of silver staining using bovine serum albumin as the protein standard.

Analysis of the disaccharide composition of various GAGs An aliquot of the GAG samples was digested with chondroitinase ABC or a mixture of recombinant heparinases I and III as described previously [30, 31]. Each digest was labeled with 2-aminobenzamide (2AB) [32], and excess 2AB reagents were removed by extraction with chloroform [33]. The 2AB-labeled digest was analyzed by anion-exchange HPLC on a PA-03 silica column (YMC Co., Kyoto, Japan) [32]. Identification and quantification of the resulting disaccharides were achieved by comparison with the elution positions of authentic unsaturated disaccharides.

Western blotting The purified E1 and E2 proteins were subjected to sodium dodecyl sulfate-polyacrylamide gel electrophoresis (SDS-PAGE) using 12.5 % polyacrylamide gels (Ready Gels J, Bio-Rad laboratories Inc., Tokyo, Japan), and transferred to a hydrophobic polyvinylidene difluoride membrane (GE Healthcare, Buckinghamshire, UK). The recombinant E1 and E2 proteins were detected with anti-V5 and anti-myc mouse monoclonal IgG antibodies (diluted 1:1,000 in 25 mM Tris-buffered saline containing 2 % blocking reagent), respectively, using Amersham ECL Advance reagents (GE Healthcare).

Enzyme-linked immunosorbent assay (ELISA) GAG preparations (250 μg) were biotinylated using EZ-Link Biotin-LC-Hydrazide as recommended by the manufacturer or Sulfo-NHS-LC-Biotin (Thermo Fisher Scientific Inc., Rockford, IL) [34]. Excess reagent was removed by dialysis against distilled water. ELISA plates (Thermo Fisher Scientific Inc.) were coated with 0.5 or 1 μg of biotinylated GAG per well at 4 °C overnight and then incubated with blocking buffer, 3 % bovine serum albumin in phosphate-buffered saline (PBS), for 1 h at room temperature. The recombinant E1 or E2 protein was added and incubated for 1 h at 37 °C. Since the molecular weight of E1 protein is approximately one sixth of that of E2 protein, the amount of the latter used was six times that of the former for the incubation to perform the assays at a similar molar concentration. After washing, the bound protein was detected by the addition of anti-V5 or anti-myc antibody (diluted 1:200 in PBS for 1 h at 37 °C) for the detection of E1 and E2, respectively, and then alkaline phosphatase-conjugated anti-mouse IgG/IgM secondary antibody (diluted 1:3,000 in Tris-buffered saline for 1 h at 37 °C). *p*-Nitrophenyl phosphate was used as the substrate for alkaline phosphatase.

For inhibition experiments, the recombinant E1 or E2 protein was preincubated for 30 min at room temperature with inhibitors (CS-E, CS-D, heparin, or heparin oligosaccharides) before being added to the biotinylated heparin-coated plate. After washing, the bound protein was detected using anti-V5 or anti-myc antibody and alkaline phosphatase-conjugated anti-mouse IgG/IgM secondary antibody as described above.

Effects of GAGs on infectivity of pseudotype vesicular stomatitis virus (VSV) possessing HCV envelope proteins (HCVpv) The construction of HCVpv and infection experiments were carried out as reported previously [35]. Briefly, HEK293T cells were transfected with an expression plasmid encoding the E1 and E2 proteins and incubated for 24 h at 37 °C. To incorporate these proteins into VSV, the cells were then infected with a VSVG-complemented pseudotype virus, in which the G envelope gene was replaced with the luciferase gene [35]. After 2 h of incubation at 37 °C, the cells were extensively washed four times with DMEM and harvested after incubation for 24 h at 37 °C. The HCVpv secreted in the conditioned medium of the infected cells was used for the infection experiment.

HCVpv was preincubated with various concentrations of CS-E, CS-D, HS, or heparin (0, 5, and 50 μg/ml) at 37 °C for 1 h and inoculated into the culture medium of Huh7 cells. After incubation for 1 h at 37 °C, the cells were washed with DMEM containing 10 % FBS three times and incubated at 37 °C for 24 h and the luciferase activity was measured.

Results

Characterization of GAGs in bovine liver tissue Hepatocytes are the main target cells of HCV. GAGs in liver tissue may contain unique structures required for the attachment of

HCV. To characterize the structural features in detail, GAGs were extracted from bovine liver, and the proportion of HS and CS/DS in GAGs derived from bovine liver was quantified to be 65 % and 35 %, respectively. HS was the major component in the GAG preparation from liver tissue. Their disaccharide composition was analyzed and the data are summarized in Tables 1 and 2. The major disaccharide unit in bovine liver HS was the trisulfated disaccharide ΔHexA (2S)-GlcN(NS, 6S) (43 %). The proportion of highly sulfated HS disaccharides (di- and trisulfated disaccharides) in bovine liver HS was 57 % (Table 1), whereas that in bovine aorta, lung, intestine, or kidney was 10 %, 21 %, 26 %, or 19 %, respectively [28], indicating the bovine liver HS to be more highly sulfated than HS from other bovine organs. The major disaccharide unit in CS/DS from bovine liver was ΔHexA-GalNAc(4S) (71 %), followed by the 4- and 6-*O*-disulfated disaccharide ΔHexA-GalNAc(4S, 6S) (25 %) (Table 2). The proportion of highly sulfated CS/DS disaccharides (di- and trisulfated disaccharides) found in the bovine liver (25 %) was significantly higher, compared with that of CS/DS preparations from bovine lung (13 %), trachea (0 %), and heart (15 %) [37, 38].

Interaction of the recombinant E1 and E2 proteins with GAGs derived from bovine liver The direct interaction of various GAGs with the recombinant E1 and E2 proteins was analyzed. HS from bovine liver, kidney, intestine, aorta, and lung as well as CS/DS from bovine liver were biotinylated and immobilized on a streptavidin-coated plate for ELISA. The recombinant proteins were produced by insect High Five cells and detected by Western blotting (Supplementary Data 1). Although their expected sizes were 10 and 40 kDa, respectively, E2 protein was larger than expected, consistent with a previous study indicating the posttranslational modification of the proteins [39]. Only bovine liver HS bound to both E1 and E2 proteins (172 % and 123 %, respectively, compared to the binding to heparin) (Fig. 1) in a concentration-dependent manner (data not shown). The interaction was confirmed using the BIAcore system. E1 and E2 proteins were individually injected at different concentrations onto the surface of the bovine liver HS-immobilized sensor chip. Overlaid sensorgrams are shown in Supplementary Data 2. Both E1 and E2 proteins bound to the bovine liver HS preparation in a concentration-dependent manner. In contrast, no significant binding of E1 or E2 to HS from other tissues or bovine liver CS/DS was observed (Fig. 1), indicating that the E1 and E2 proteins interact specifically with bovine liver HS, which appears to play the major role in the binding of HCV to liver cells, in consistent with the tissue tropism of the infection of HCV.

Determination of the sulfation structure required for the binding to E1 and E2 proteins To study whether the binding of the E1 and E2 proteins to heparin requires structurally defined HS oligosaccharides, the size effect of heparin oligosaccharides (ranging from di- to dodecasaccharides and polysaccharides) on the binding of E1 or E2 to immobilized heparin was analyzed. Although the reactivity of the E1 and E2 proteins with the immobilized heparin was strongly inhibited by free heparin polysaccharide chains, heparin oligosaccharides did not exhibit as much inhibitory activity as heparin polysaccharides. However, the 10-mer and 12-mer forms showed some inhibition (Fig. 2), indicating the minimum length required for the inhibition to be 10-mer. This result is consistent with a report that HCV pseudoparticles required heparin oligosaccharides of at least 10-mer for binding [40].

The structure required for the binding was characterized further. Chemically modified heparin derivatives were used to analyze the direct interaction. Both the E1 and E2 proteins bound strongly to *2ODS* (84 % and 58 %, respectively, compared to the binding to heparin) and moderately to *6ODS* (38 % and 23 %) and *NDNA* (34 % and 19 %), whereas no significant interaction of either protein with *CDNS* or *CDNA* was observed (Fig. 3), indicating that sulfation at the C2 (amino group) and C6 positions of GlcN residues is more important for the interaction than sulfation at the C2 position of uronic acid residues.

Table 1 Disaccharide composition of HS derived from various tissues (%)

	ΔHexA-GlcNAc	ΔHexA-GlcN(NS)	ΔHexA-GlcNAc(6S)	ΔHexA (2S)-GlcNAc	ΔHexA-GlcN(NS, 6S)	ΔHexA(2S)-GlcN(NS)	ΔHexA(2S)-GlcNAc(6S)	ΔHexA(2S)-GlcN(NS, 6S)	S/unit[b]	Ref. No.
Bovine Aorta	63	20	6	1	2	5	ND	3	0.50	28
Bovine Lung	45	16	17	1	9	8	ND	4	0.80	28
Bovine Intestine	45	19	9	1	8	11	ND	7	0.88	28
Bovine Kidney	53	16	11	1	6	7	ND	6	0.72	28
Bovine Liver	20	17	6	ND[a]	8	3	3	36	1.80	–
Human Liver	37	15	10	1	8	6	1	22	1.22	36

[a] *ND* not detected

[b] *S/unit* the number of sulfate groups per disaccharide unit

Table 2 Disaccharide composition of bovine liver CS/DS

CS/DS disaccharide	Proportion (%)
ΔHexA-GalNAc	ND[a]
ΔHexA-GalNAc(6S)	4
ΔHexA-GalNAc(4S)	71
ΔHexA(2S)-GalNAc(6S)	ND
ΔHexA(2S)-GalNAc(4S)	ND
ΔHexA-GalNAc(4S, 6S)	25
ΔHexA(2S)-GalNAc(4S, 6S)	ND
S/unit[b]	1.25

[a] *ND* not detected

[b] *S/unit* the number of sulfate groups per disaccharide unit

Effect of highly sulfated CS preparations on the infectivity of pesudotype HCV Since a highly sulfated structure is required for interaction with the E1 and E2 proteins, some CS preparations derived from marine animals, which are more highly sulfated than those from mammalian tissue, may bind the proteins. To investigate the potential of such highly sulfated CS from marine animals to inhibit the entry of HCV into host cells, effects on the infection by pesudotype HCV (HCVpv) of Huh7 cells were examined. Highly sulfated CS (CS-D and CS-E), heparin, and bovine liver HS preparations showed dose-dependent inhibition of HCVpv infection, whereas no significant effect was observed on the addition of low sulfated HS from bovine kidney (Fig. 4), indicating that highly sulfated CS and HS/heparin can inhibit the infection of Huh7 cells by HCVpv.

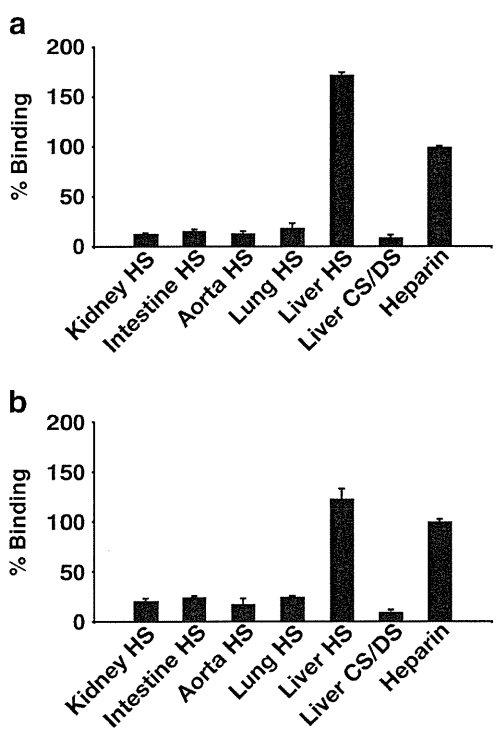

Fig. 1 Interaction of the recombinant E1 or E2 protein with GAGs from various bovine tissues. ELISA plates were coated with 1 μg/well of biotinylated GAGs from various bovine tissues or porcine intestinal heparin as described under "Materials and methods". Recombinant E1 (**a**) or E2 (**b**) protein (3 or 18 μg, respectively) was added and incubated for 1 h at 37 °C. After a wash with PBS/0.05 % Tween 20, the bound E1 and E2 proteins were detected using monoclonal anti-V5 and anti-myc antibodies, respectively, and then alkaline phosphatase-conjugated anti-mouse IgG/IgM secondary antibody. Data are shown as a percentage of the binding of the E1 or E2 protein to heparin. Values represent the mean±standard deviation (SD) (n=2)

Interaction of the recombinant E1 and E2 proteins with highly sulfated CS preparations To examine whether the highly sulfated CS preparations (CS-D and CS-E) bind directly to the recombinant E1 and E2 proteins, the interaction of the proteins with immobilized CS-D and CS-E was examined. Both the E1 and E2 proteins bound strongly to CS-E (69 % and 85 %, respectively, compared to heparin), but very weakly to CS-D (4 % and 19 %, respectively) (Fig. 5). These results may reflect the difference in their total negative charge as represented by the number of sulfate groups per disaccharide unit. CS-D and CS-E contain 1.2 and 1.6 sulfate groups per disaccharide [41], respectively. To further characterize the binding of the recombinant E1 and E2 proteins to highly sulfated CS, the inhibitory effect of CS-E and CS-D on the binding of the E1 and E2 proteins to immobilized heparin was examined. The binding to E1 or E2 was weakly inhibited by CS-D and CS-E or CS-D, respectively (11 % and 22 % or 31 % inhibition at 10 μg/well, respectively, compared to the binding in the absence of inhibitors), whereas the binding to E2 was strongly inhibited by CS-E (54 % inhibition at 5 μg/well, compared to the binding in the absence of inhibitors) (Fig. 6), supporting the higher affinity of CS-E than CS-D for the E1 and E2 proteins.

Discussion

Several lines of evidence have demonstrated that GAGs play an important role in the attachment of HCV to host cells [3, 12, 13, 40]. Among GAGs, heparin has been well studied for its interaction with the envelope glycoproteins E1 and E2 [3, 40]. Heparin is distributed in the cytoplasmic granules of mast cells *in vivo* and more highly sulfated than HS, which is ubiquitous on the cell surface [42]. HS at the cell surface in human liver was predicted to interact with the HCV envelope proteins based on reports by Barth *et al.* [3, 40, 43]. However, no direct interaction between the viral proteins and GAGs derived from liver tissue has been shown. In this study, we characterized the disaccharide composition of the GAGs derived from bovine liver and demonstrated the direct interaction of the highly sulfated HS from bovine liver with both E1 and E2 proteins for the first time, although Barth *et al.* have demonstrated inhibition of the cellular binding of E1 and E2 proteins to human

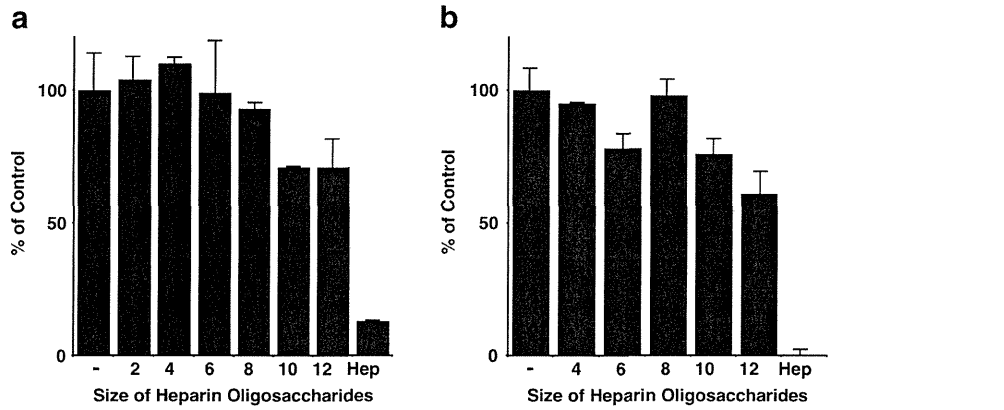

Fig. 2 Inhibition of the interaction of the E1 or E2 protein with heparin by heparin oligosaccharides. The E1 (**a**) or E2 (**b**) protein (0.75 or 4.5 μg, respectively) was preincubated with size-defined heparin oligosaccharides ranging from di- to dodecasaccharides and polysaccharides (15 μg each) for 30 min at room temperature and then the mixture was added to an ELISA plate coated with biotinylated heparin (0.5 μg per well). The bound E1 and E2 proteins were detected using anti-V5 and anti-myc antibodies, respectively. Data are shown as a percentage of the binding in the absence of heparin oligosaccharides. Values represent the mean±SD (n=2)

hepatoma cell lines by liver-derived HS [40]. Intriguingly, among the HS preparations from various tissues, only liver HS bound to E1 and E2 proteins strongly. Since HS from human liver, which is the target tissue of HCV, contains highly sulfated structures (di- and trisulfated disaccahrides) accounting for 37 % of all disaccharides (Table 1) [36], the present results provide further evidence that HCV utilizes cellular HS for attachment to the target tissue. HS-PG on the liver cell surface appears to be one of the molecules that define the liver-specific tissue tropism of HCV, in addition to the internal ribosome entry site (IRES)-dependent HCV tropism [44]. The participation of HS in virus tropism to different tissues has been suggested [21, 45].

Although bovine liver HS was used for the interaction with the E1 and E2 proteins, HCV infects only human and chimpanzee but not bovine liver. The species tropism of HCV is modulated at the level of cell entry, and recently it has been reported that the expression of CD81 and occludin, which are important for HCV entry, is sufficient to allow the HCV infection of mice [46]. Since the primary structure of HS is common among mammals, and liver HS is generally highly sulfated [47], HS in liver is likely involved in the enrichment of HCV particles before or together with CD81 and/or occludin.

The recombinant E1 and E2 proteins prepared in this study were the ectodomain of the viral envelope proteins. They are truncated immediately upstream its transmembrane region, and soluble. The recombinant E1 and E2 proteins have been suggested to adopt a native conformation based on the interaction with conformation-sensitive monoclonal antibodies as well as inhibition of the infection

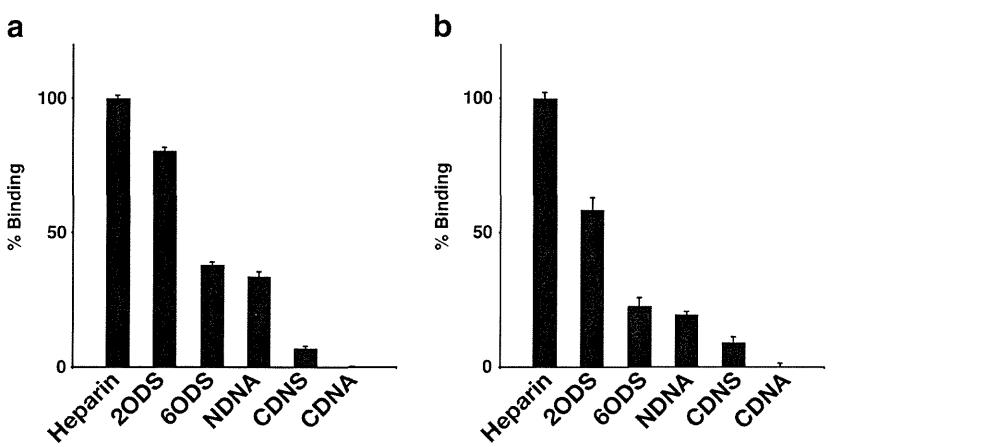

Fig. 3 Interaction of the E1 or E2 protein with chemically modified heparin preparations. ELISA plates were coated with biotinylated heparin derivatives, *CDNS*, *CDNA*, *NDNA*, *2ODS*, *6ODS*, or unmodified heparin (1 μg each per well). The recombinant E1 (**a**) or E2 (**b**) protein (0.75 or 4.5 μg, respectively) was added and incubated for 1 h at 37 °C. The bound E1 or E2 protein was detected using monoclonal anti-V5 or anti-myc antibody. Data are shown as a percentage of the binding of the E1 or E2 protein to unmodified heparin. Values represent the mean±SD (n=2)

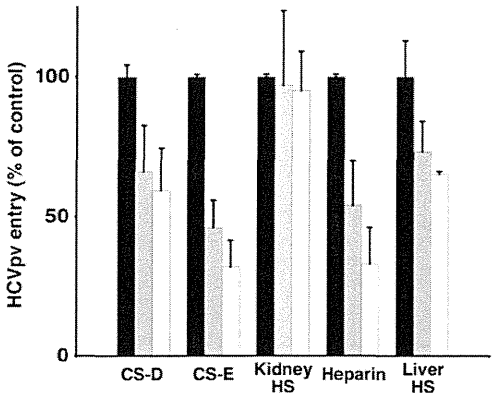

Fig. 4 Effect of highly sulfated CS on the infectivity of pesudotype HCV (HCVpv) to Huh7 cells. HCVpv was preincubated with CS-D, CS-E, HS, or heparin at a concentration of 0 μg/ml (closed columns), 5 μg/ml (hatched columns), and 50 μg/ml (open columns) for 1 h at 37 °C, and the mixture was added to the culture medium of Huh7 cells. After 2 h of incubation at 37 °C, the cells were washed three times with DMEM containing 10 % FBS, and the luciferase activity was measured after 24 h. Data are shown as a percentage of the infectivity of HCVpv to Huh7 cells in the absence of GAGs. Values represent the mean±SD (n=3)

of Huh 7.5 cells by infectious HCV particles [48]. However, the conformation of the recombinant soluble proteins might be different to some extent from that of the native proteins, because liver HS, which shows higher affinity to the recombinant proteins (Fig. 1), was less effective in the inhibition of the infection by HCVpv (Fig. 4) than heparin.

The binding of GAGs to viral proteins is mediated by simple effects of charge and/or highly specific interactions as described for HS [20]. The interaction of E1 and E2 with bovine liver GAGs or chemically modified heparin derivatives provides evidence that the binding of the viral proteins to heparin/HS is not only mediated by simple interactions, but most likely includes a specific interaction with a defined structure present in HS. *2ODS* bound strongly to both E1 and E2, whereas neither *6ODS* nor *NDNA* heparin derivatives did in spite of their similar degree of sulfation (approximately 1.6 sulfate groups per disaccharide unit), indicating the importance of 6-*O*-sulfation and *N*-sulfation in the binding of the proteins. Bovine liver HS (1.80 sulfate groups per disaccharide unit), which is not as highly sulfated as heparin (2.40 sulfate groups per disaccharide unit), bound at least as strongly to the viral proteins as heparin. Barth *et al.* [40] observed that de-*N*-sulfated heparin lost its inhibitory effect on the binding of the E1 and E2 proteins to heparin, while neither de-2-*O*- nor de-6-*O*-sulfated heparin did, suggesting that *N*-sulfation but neither 2-*O*- nor 6-*O*-sulfations is important for the interaction with the viral proteins. This difference in the specificity with which heparin binds to the viral proteins may be due to the experimental design (assays of inhibition or direct interaction). Different methods of preparing the chemically modified heparin derivatives may also be a cause.

The size of the saccharides also seemed to be important in the binding of E1 and E2 to heparin. No significant inhibition of the binding of the proteins to immobilized heparin was shown by heparin oligosaccharides shorter than 10-mer, indicating that a length of at least 10-mer is required for the binding. However, even long oligosaccharides (up to 20-mer) did not exhibit as much inhibitory effect as heparin polysaccharides (data not shown). The longer their chains become, the more effectively oligosaccharides appear to inhibit the binding of E1 or E2 to the immobilized heparin.

CS/DS derived from bovine liver, which is more highly sulfated than CS/DS from other organs [17], bound to neither E1 nor E2. Although both highly sulfated CS/DS and HS are expressed in liver, only the latter specifically bound to E1 and E2 (Fig. 1). It has been demonstrated that treatment of the host cells with heparinase but not with chondroitinase

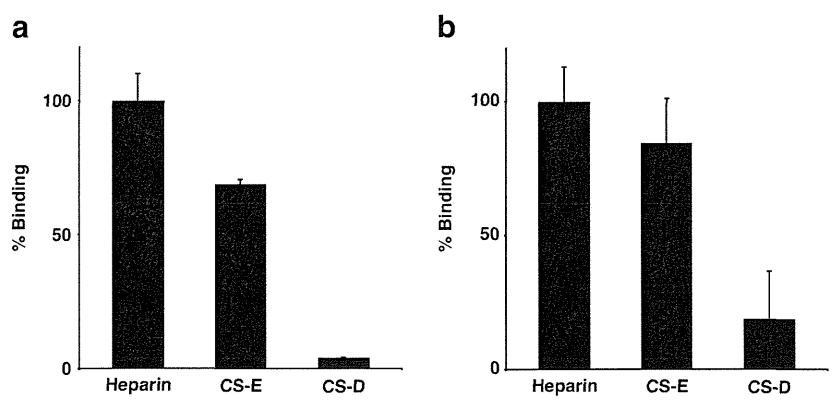

Fig. 5 Interaction of the recombinant E1 or E2 protein with highly sulfated CS preparations. ELISA plates were coated with 0.5 μg/well of biotinylated heparin, CS-E, or CS-D as described under "Materials and methods". The recombinant E1 (**a**) or E2 (**b**) protein (0.75 or 4.5 μg, respectively) was added and incubated for 1 h at 37 °C. The bound E1 and E2 proteins were detected using monoclonal anti-V5 and anti-myc antibodies, respectively. Data are shown as a percentage of the binding of the E1 or E2 protein to heparin. Values represent the mean±SD (n=2)

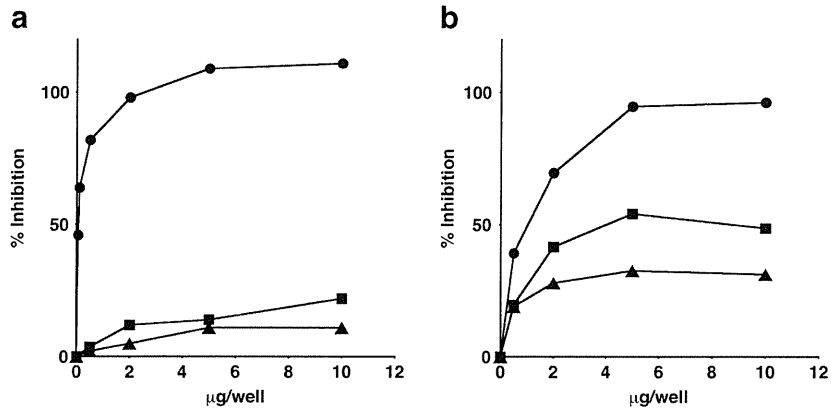

Fig. 6 Inhibition of the binding of biotinylated heparin to the recombinant E1 or E2 protein by CS-E, CS-D, and heparin. The recombinant E1 (**a**) or E2 (**b**) protein (1.2 or 3.6 μg, respectively) was preincubated with CS-D (triangles), CS-E (squares), or heparin (circles) (0, 0.05, 0.1, 0.5, 2, 5, or 10 μg per well) for 30 min at 37 °C and then added to an ELISA plate coated with biotinylated heparin (0.5 μg per well). The bound E1 or E2 protein was detected using monoclonal anti-V5 or anti-myc antibody, respectively. Data are shown as percent inhibition of the binding of the E1 or E2 protein to biotinylated heparin in the absence of inhibitors. Values represent the mean (n=2)

ABC reduced the infectivity of pseudotype HCV, suggesting the importance of HS on the host cell surface for the infection [49]. In contrast to HS, CS/DS seems to contribute little to the cellular attachment of HCV at least in liver tissue. It, however, has not been clarified whether CS/DS from human liver tissue contains a highly sulfated CS-E-like structure that can bind to the HCV envelope proteins.

Highly sulfated CS from marine animals, CS-E and CS-D (1.6 and 1.2 sulfate groups per disaccharide unit, respectively), interacted with both viral proteins (Fig. 5). Since highly sulfated heparin derivatives (*6ODS* and *NDNA*; 1.6 sulfate groups per disaccharide unit) bound only weakly to the viral proteins (Fig. 3), the interaction of the two viral proteins with GAGs may be mediated by not only simple charge effects but also by defined sulfated structures. CS-D and CS-E also inhibited the entry of pseudotype HCV into the target cells (Fig. 4), suggesting the potential medical application of these highly sulfated CS as an anti-HCV drug.

HS-PG in the extracellular matrix is known to function as a reservoir for various growth factors including fibroblast growth factors (FGFs) and prevent proteases from degrading the growth factors [50, 51]. Liver HS may also hold HCV particles and protect them from attack by the immune system of the host. HCV may be concentrated at the liver cell surface through interaction with membrane-bound HS-PG, leading to an acceleration of the infection. The FGF receptor has been revealed to be involved in infections by HCV (Matsuura, Y. *et al.*, unpublished data). The ternary complex formed by HS, FGF, and the FGF receptor has been well investigated, and demonstrated to be required for the mitogenic effects of FGFs [18, 52, 53]. HCV may also be able to form a ternary complex with HS and the FGF receptor. To investigate this possibility, we performed competition ELISA experiments. The binding of E1 and E2 proteins with heparin was inhibited by the addition of basic FGF in a dose-dependent manner (results not shown), indicating that basic FGF and the viral proteins recognize the same or partially overlaping saccharide sequences in heparin. Determination of the sequences in GAGs specific for the binding to E1 and E2 proteins is required for characterization of their interaction to develop anti-HCV drugs.

Acknowledgments The authors thank Satoko Ueno, Naoko Shoji, and Machiko Tomimatsu for technical assistance. This work was supported in part by Grants-in-aid for Scientific Research C-21590057 (to S. Y.), Scientific Research (B) 23390016 (to K. S.), and the Matching Program for Innovations in Future Drug Discovery and Medical Care (to K. S.) from the Ministry of Education, Culture, Sports, Science, and Technology of Japan (MEXT).

References

1. Wasley, A., Alter, M.J.: Epidemiology of hepatitis C: geographic differences and temporal trends. Semin. Liver Dis. **20**, 1–16 (2000)
2. Lauer, G.M., Walker, B.D.: Hepatitis C virus infection. N. Engl. J. Med. **345**, 41–52 (2001)
3. Barth, H., Schafer, C., Adah, M.I., Zhang, F., Linhardt, R.J., Toyoda, H., Kinoshita-Toyoda, A., Toida, T., Van Kuppevelt, T.H., Depla, E., Von Weizsacker, F., Blum, H.E., Baumert, T.F.: Cellular binding of hepatitis C virus envelope glycoprotein E2 requires cell surface heparan sulfate. J. Biol. Chem. **278**, 41003–41012 (2003)
4. Koutsoudakis, G., Kaul, A., Steinmann, E., Kallis, S., Lohmann, V., Pietschmann, T., Bartenschlager, R.: Characterization of the early steps of hepatitis C virus infection by using luciferase reporter viruses. J. Virol. **80**, 5308–5320 (2006)
5. Agnello, V., Abel, G., Elfahal, M., Knight, G.B., Zhang, Q.X.: Hepatitis C virus and other flaviviridae viruses enter cells via low density lipoprotein receptor. Proc. Natl. Acad. Sci. U. S. A. **96**, 12766–12771 (1999)
6. Monazahian, M., Böhme, I., Bonk, S., Koch, A., Scholz, C., Grethe, S., Thomssen, R.: Low density lipoprotein receptor as a candidate receptor for hepatitis C virus. J. Med. Virol. **57**, 223–229 (1999)

7. Pileri, P., Uematsu, Y., Campagnoli, S., Galli, G., Falugi, F., Petracca, R., Weiner, A.J., Houghton, M., Rosa, D., Grandi, G., Abrignani, S.: Binding of hepatitis C virus to CD81. Science **282**, 938–941 (1998)
8. Bartosch, B., Vitelli, A., Granier, C., Goujon, C., Dubuisson, J., Pascale, S., Scarselli, E., Cortese, R., Nicosia, A., Cosset, F.L.: Cell entry of hepatitis C virus requires a set of co-receptors that include the CD81 tetraspanin and the SR-B1 scavenger receptor. J. Biol. Chem. **278**, 41624–41630 (2003)
9. Evans, M.J., von Hahn, T., Tscherne, D.M., Syder, A.J., Panis, M., Wölk, B., Hatziioannou, T., McKeating, J.A., Bieniasz, P.D., Rice, C.M.: Claudin-1 is a hepatitis C virus co-receptor required for a late step in entry. Nature **446**, 801–805 (2007)
10. Liu, S., Yang, W., Shen, L., Turner, J.R., Coyne, C.B., Wang, T.: Tight junction proteins claudin-1 and occludin control hepatitis C virus entry and are downregulated during infection to prevent superinfection. J. Virol. **83**, 2011–2014 (2009)
11. Moradpour, D., Penin, F., Rice, C.M.: Replication of hepatitis C virus. Nat. Rev. Microbiol. **5**, 453–463 (2007)
12. Garson, J.A., Lubach, D., Passas, J., Whitby, K., Grant, P.R.: Suramin blocks hepatitis C binding to human hepatoma cells in vitro. J. Med. Virol. **57**, 238–242 (1999)
13. Liu, B., Paranjpe, S., Bowen, W.C., Bell, A.W., Luo, J.H., Yu, Y.P., Mars, W.M., Michalopoulos, G.K.: Investigation of the role of glypican 3 in liver regeneration and hepatocyte proliferation. Am. J. Pathol. **175**, 717–724 (2009)
14. Yagnik, A.T., Lahm, A., Meola, A., Roccasecca, R.M., Ercole, B.B., Nicosia, A., Tramontano, A.: A model for the hepatitis C virus envelope glycoprotein E2. Proteins **40**, 355–366 (2000)
15. Sugahara, K., Kitagawa, H.: Recent advances in the study of the biosynthesis and functions of sulfated glycosaminoglycans. Curr. Opin. Struct. Biol. **10**, 518–527 (2000)
16. Esko, J.D., Selleck, S.B.: Order out of chaos: assembly of ligand binding sites in heparan sulfate. Annu. Rev. Biochem. **71**, 435–471 (2001)
17. Yamada, S., Sugahara, K.: Potential therapeutic application of chondroitin sulfate/dermatan sulfate. Curr. Drug Discov. Tech. **5**, 289–301 (2008)
18. Casu, B., Lindahl, U.: Structure and biological interactions of heparin and heparan sulfate. Adv. Carbohydr. Chem. Biochem. **57**, 159–206 (2001)
19. Kreuger, J., Spillmann, D., Li, J.P., Lindahl, U.: Interactions between heparan sulfate and proteins: the concept of specificity. J. Cell Biol. **174**, 323–327 (2006)
20. Shukla, D., Spear, P.G.: Herpesviruses and heparan sulfate: an intimate relationship in aid of viral entry. J. Clin. Invest. **108**, 503–510 (2001)
21. Spillmann, D.: Heparan sulfate: anchor for viral intruders? Biochimie **83**, 811–817 (2001)
22. Rostand, K.S., Esko, J.D.: Microbial adherence to and invasion through proteoglycans. Infect. Immun. **65**, 1–8 (1997)
23. Giroglou, T., Florin, L., Schäfer, F., Streeck, R.E., Sapp, M.: Human papillomavirus infection requires cell surface heparan sulfate. J. Virol. **75**, 1565–1570 (2001)
24. Birkmann, A., Mahr, K., Ensser, A., Yağuboğlu, S., Titgemeyer, F., Fleckenstein, B., Neipel, F.: Cell surface heparan sulfate is a receptor for human herpesvirus 8 and interacts with envelope glycoprotein K8.1. J. Virol. **75**, 11583–11593 (2001)
25. Liu, J., Thorp, S.C.: Cell surface heparan sulfate and its roles in assisting viral infections. Med. Res. Rev. **22**, 1–25 (2002)
26. Ishihara, M., Takano, R., Kanda, T., Hayashi, K., Hara, S., Kikuchi, H., Yoshida, K.: Importance of 6-*O*-sulfate groups of glucosamine residues in heparin for activation of FGF-1 and FGF-2. J. Biochem. **118**, 1255–1260 (1995)
27. Ishihara, M., Kariya, Y., Kikuchi, H., Minamisawa, T., Yoshida, K.: Importance of 2-*O*-sulfate groups of uronate residues in heparin for activation of FGF-1 and FGF-2. J. Biochem. **121**, 345–349 (1997)
28. Maccarana, M., Sakura, Y., Tawada, A., Yoshida, K., Lindahl, U.: Domain structure of heparan sulfates from bovine organs. J. Biol. Chem. **271**, 17804–17810 (1996)
29. Yamane, Y., Tohno-oka, R., Yamada, S., Furuya, S., Shiokawa, K., Hirabayashi, Y., Sugino, H., Sugahara, K.: Molecular characterization of *Xenopus* embryo heparan sulfate. Differential structural requirements for the specific binding to basic fibroblast growth factor and follistatin. J. Biol. Chem. **273**, 7375–7381 (1998)
30. Ueno, M., Yamada, S., Zako, M., Bernfield, M., Sugahara, K.: Structural characterization of heparan sulfate and chondroitin sulfate of syndecan-1 purified from normal murine mammary gland epithelial cells. Common phosphorylation of xylose and differential sulfation of galactose in the protein linkage region tetrasaccharide sequence. J. Biol. Chem. **276**, 29134–29140 (2001)
31. Nandini, C.D., Itoh, N., Sugahara, K.: Novel 70-kDa chondroitin sulfate/dermatan sulfate hybrid chains with a unique heterogeneous sulfation pattern from shark skin, which exhibit neuritogenic activity and binding activities for growth factors and neurotrophic factors. J. Biol. Chem. **280**, 4058–4069 (2005)
32. Kinoshita, A., Sugahara, K.: Microanalysis of glycosaminoglycan-derived oligosaccharides labeled with the fluorophore 2-aminobenzamide by high-performance liquid chromatography: application to disaccharide composition analysis and exo-sequencing of oligosaccharides. Anal. Biochem. **269**, 367–378 (1999)
33. Kawashima, H., Atarashi, K., Hirose, M., Hirose, J., Yamada, S., Sugahara, K., Miyasaka, M.: Oversulfated chondroitin/dermatan sulfates containing GlcAβ1/IdoAα1-3GalNAc(4,6-*O*-disulfate) interact with L- and P-selectin and chemokines. J. Biol. Chem. **277**, 12921–12930 (2002)
34. Saito, A., Munakata, H., Satoh, K.: Glyco-western blotting: biotinylated dermatan sulfate as a probe for the detection of dermatan sulfate binding proteins using western blotting. Connect. Tissue Res. **43**, 1–7 (2002)
35. Tani, H., Komoda, Y., Matsuo, E., Suzuki, K., Hamamoto, I., Yamashita, T., Moriishi, K., Fujiyama, K., Kanto, T., Hayashi, N., Owsianka, A., Patel, A.H., Whitt, M.A., Matsuura, Y.: Replication-competent recombinant vesicular stomatitis virus encoding hepatitis C virus envelope proteins. J. Virol. **81**, 8601–8612 (2007)
36. Vongchan, P., Warda, M., Toyoda, H., Toida, T., Marks, R.M., Linhardt, R.J.: Structural characterization of human liver heparan sulfate. Biochim. Biophys. Acta **1721**, 1–8 (2005)
37. Volpi, N.: Disaccharide analysis and molecular mass determination to microgram level of single sulfated glycosaminoglycan species in mixtures following agarose-gel electrophoresis. Anal. Biochem. **273**, 229–239 (1999)
38. Volpi, N.: Hyaluronic acid and chondroitin sulfate unsaturated disaccharides analysis by high-performance liquid chromatography and fluorimetric detection with dansylhydrazine. Anal. Biochem. **277**, 19–24 (2000)
39. Matsuura, Y., Harada, S., Suzuki, R., Watanabe, Y., Inoue, Y., Saito, I., Miyamura, T.: Expression of processed envelope protein of hepatitis C virus in mammalian and insect cells. J. Virol. **66**, 1425–1431 (1992)
40. Barth, H., Schnober, E.K., Zhang, F., Linhardt, R.J., Depla, E., Boson, B., Cosset, F.L., Patel, A.H., Blum, H.E., Baumert, T.F.: Viral and cellular determinants of the hepatitis C virus envelope-heparan sulfate interaction. J. Virol. **80**, 10579–10590 (2006)
41. Li, F., Yamada, S., Basappa, Shetty, A.K., Sugiura, M., Sugahara, K.: Determination of iduronic acid and glucuronic acid in sulfated chondroitin/dermatan hybrid chains by ^{1}H-nuclear magnetic resonance spectroscopy. Glycoconj. J. **25**, 603–610 (2008)
42. Salmivirta, M., Lidholt, K., Lindahl, U.: Heparan sulfate: a piece of information. FASEB J. **10**, 1270–1279 (1996)

43. Barth, H., Liang, T.J., Baumert, T.F.: Hepatitis C virus entry: molecular biology and clinical implications. Hepatology **44**, 527–535 (2006)
44. Yanagiya, A., Ohka, S., Hashida, N., Okamura, M., Taya, C., Kamoshita, N., Iwasaki, K., Sasaki, Y., Yonekawa, H., Nomoto, A.: Tissue-specific replicating capacity of a chimeric poliovirus that carries the internal ribosome entry site of hepatitis C virus in a new mouse model transgenic for the human poliovirus receptor. J. Virol. **77**, 10479–10487 (2003)
45. Bergström, T., Trybala, E., Spillmann, D.: Heparan sulfate and viral tropism. Nat. Med. **3**, 1177 (1997)
46. Dorner, M., Horwitz, J.A., Robbins, J.B., Barry, W.T., Feng, Q., Mu, K., Jones, C.T., Schoggins, J.W., Catanese, M.T., Burton, D.R., Law, M., Rice, C.M., Ploss, A.: A genetically humanized mouse model for hepatitis C virus infection. Nature **474**, 208–211 (2011)
47. Lyon, M., Deakin, J.A., Gallagher, J.T.: Liver heparan sulfate structure. A novel molecular design. J. Biol. Chem. **269**, 11208–11215 (1994)
48. Krey, T., d'Alayer, J., Kikuti, C.M., Saulnier, A., Damier-Piolle, L., Petitpas, I., Johansson, D.X., Tawar, R.G., Baron, B., Robert, B., England, P., Persson, M.A., Martin, A., Rey, F.A.: The disulfide bonds in glycoprotein E2 of hepatitis C virus reveal the tertiary organization of the molecule. PLoS Pathog. **6**, e1000762 (2010)
49. Matsuura, Y., Tani, H., Suzuki, K., Kimura-Someya, T., Suzuki, R., Aizaki, H., Ishii, K., Moriishi, K., Robison, C.S., Whitt, M.A., Miyamura, T.: Characterization of pseudotype VSV possessing HCV envelope proteins. Virology **286**, 263–275 (2001)
50. Gospodarowicz, D., Cheng, J.: Heparin protects basic and acidic FGF from inactivation. J. Cell. Physiol. **128**, 475–484 (1986)
51. Powers, C.J., McLeskey, S.W., Wellstein, A.: Fibroblast growth factors, their receptors and signaling. Endocr. Relat. Canc. **7**, 165–197 (2000)
52. Fernig, D.G., Gallagher, J.T.: Fibroblast growth factors and their receptors: an information network controlling tissue growth, morphogenesis and repair. Progr. Growth Factor Res. **5**, 353–377 (1994)
53. Mohammadi, M., Olsen, S.K., Goetz, R.: A protein canyon in the FGF-FGF receptor dimer selects from an à la carte menu of heparan sulfate motifs. Curr. Opin. Struct. Biol. **15**, 506–516 (2005)

Journal of proteome research

Article

pubs.acs.org/jpr

Proteomic Analysis of Hepatitis C Virus (HCV) Core Protein Transfection and Host Regulator PA28γ Knockout in HCV Pathogenesis: A Network-Based Study

Lokesh P. Tripathi,[†,∥] Hiroto Kambara,[‡,∥] Kohji Moriishi,[‡] Eiji Morita,[‡] Takayuki Abe,[‡] Yoshio Mori,[‡] Yi-An Chen,[†,§] Yoshiharu Matsuura,[‡] and Kenji Mizuguchi*[,†,§]

[†]National Institute of Biomedical Innovation, 7-6-8 Saito Asagi, Ibaraki, Osaka, 567-0085, Japan

[‡]Department of Molecular Virology, Research Institute for Microbial Diseases and [§]Graduate School of Frontier Biosciences, Osaka University, 3-1 Yamada-Oka, Suita, Osaka, 565-0871, Japan

S *Supporting Information*

ABSTRACT: Hepatitis C virus (HCV) causes chronic liver disease worldwide. HCV Core protein (Core) forms the viral capsid and is crucial for HCV pathogenesis and HCV-induced hepatocellular carcinoma, through its interaction with the host factor proteasome activator PA28γ. Here, using BD-PowerBlot high-throughput Western array, we attempt to further investigate HCV pathogenesis by comparing the protein levels in liver samples from Core-transgenic mice with or without the knockout of PA28γ expression (abbreviated PA28γ$^{-/-}$CoreTG and CoreTG, respectively) against the wild-type (WT). The differentially expressed proteins integrated into the human interactome were shown to participate in compact and well-connected cellular networks. Functional analysis of the interaction networks using a newly developed data warehouse system highlighted cellular pathways associated with vesicular transport, immune system, cellular adhesion, and cell growth and death among others that were prominently influenced by Core and PA28γ in HCV infection. Follow-up assays with *in vitro* HCV cell culture systems validated VTI1A, a vesicular transport associated factor, which was upregulated in CoreTG but not in PA28γ$^{-/-}$CoreTG, as a novel regulator of HCV release but not replication. Our analysis provided novel insights into the Core-PA28γ interplay in HCV pathogenesis and identified potential targets for better anti-HCV therapy and potentially novel biomarkers of HCV infection.

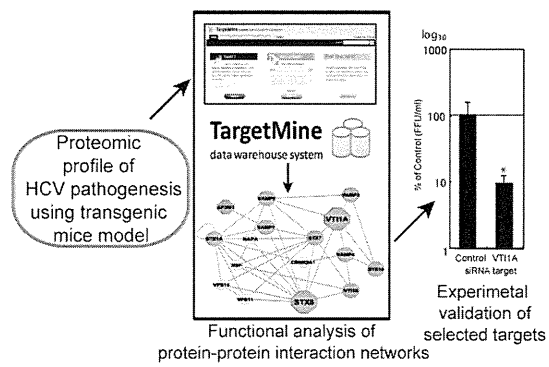

KEYWORDS: *CoreTG, GO, HCC, HCV, KEGG, OMIM, PA28γ$^{-/-}$CoreTG, PPI, siRNA, TargetMine*

INTRODUCTION

Hepatitis C virus (HCV) is a prime cause of chronic liver disease frequently characterized by liver inflammation with accompanying steatosis, progressive fibrosis, and hepatocellular carcinoma (HCC) and infects nearly 3% of the world's population. HCV contains a single-stranded RNA genome encoding a 3000-amino-acid polyprotein, which is processed by host and viral factors to yield 10 viral proteins, Core, E1, E2, p7, NS2, NS3, NS4A, NS4B, NS5A, and NS5B.[1−4] HCV variants are classified into six major genotypes with multiple subtypes characterized by phylogenetic heterogeneity, differences in infectivity, and interferon sensitivity.[5,6] The availability of cell-culture-based systems for HCV infection has provided an increased understanding of HCV pathogenesis.[5,7−9] Transgenic mice (preferably C57BL strain) expressing HCV proteins in the liver are also a preferred choice for the investigation of HCV pathogenesis.[10] However, despite considerable research efforts, precise molecular mechanisms underlying HCV pathology remain unclear.

HCV Core protein (hereafter referred to as Core) is spliced from the polyprotein by the signal peptidase and further processed into a highly conserved 21-kDa mature form by the signal peptide peptidase; this processing facilitates its transfer to the detergent-resistant membrane fraction where virus replication and assembly take place. Core is a multifunctional protein implicated in RNA binding and as a pathogenic factor; it induces steatosis and HCC and, thus, liver failure.[1,10] The ubiquitin-proteasome pathway, the premier intracellular protein degradation system in eukaryotes, is a key regulator of cellular processes and is also associated with the evasion of host immune response by many viruses, viral maturation, and progeny release.[11] Core binds to the proteasome activator PA28γ in the nucleus and is degraded via a PA28γ-dependent pathway. PA28γ plays a crucial role in Core-induced insulin resistance, steatogenesis, and hepatocarcinogenesis and in HCV propagation; PA28γ knockout in Core transgenic mice disrupts

Received: February 7, 2012
Published: May 31, 2012

steatosis and HCC, restores insulin sensitivity, and impairs viral particle production, and thus PA28γ is a promising target for anti-HCV therapies with minimal side effects.[2,12−15] However, the exact mechanisms through which PA28γ facilitates Core-induced HCV pathogenesis remain poorly understood.

In this study, we aim to put forth biological networks that describe the differential expression of the host proteins and their likely roles in modulating PA28γ function in HCV pathogenesis. We employed PowerBlot Western Array screening system, a high-throughput Western blotting method, to identify changes at the proteome level in Core expressing transgenic C57BL/6 mice with or without the knockout of PA28γ gene expression (abbreviated PA28$\gamma^{-/-}$CoreTG and CoreTG, respectively). In our analysis, we included human protein interaction data and gene regulatory information for the differentially expressed proteins using TargetMine, an integrated data warehouse that we have developed recently.[16] Our network-based analyses of the proteomic changes from the three data sets (CoreTGvsC57BL/6, PA28$\gamma^{-/-}$CoreTGvsC57BL/6 and PA28$\gamma^{-/-}$CoreTGvsCoreTG) provided novel insights into PA28γ function in Core-induced HCV pathogenesis. Furthermore, we identified VTI1A, a vesicular transport associated factor, which was upregulated in CoreTG but not in PA28$\gamma^{-/-}$CoreTG, as a novel regulator of HCV release and, thus, an attractive target for anti-HCV therapy.

MATERIALS AND METHODS

Protein Sample Preparation

Protein samples were prepared from the livers of the C57BL/6 wild-type (hereafter referred to as WT) and the transgenic mice expressing HCV Core protein genotype 1b line C49 with (PA28$\gamma^{-/-}$CoreTG) or without (CoreTG) the knockout of PA28γ expression.[2,12] Livers were harvested from three individuals each of WT, CoreTG, and PA28$\gamma^{-/-}$CoreTG mice, and the harvested samples for each mice type were pooled together prior to protein sample preparation for PowerBlot analysis. The pooled liver samples of each mice type were homogenized in 1x sample buffer of SDS-PAGE on ice and then boiled for 5 min. The boiled sample was sonicated for the viscosity of DNA and employed for PowerBlot analysis.

PowerBlot Western Array Analysis

The levels of differentially expressed proteins were determined by the PowerBlot assay by BD Biosciences Pharmingen (San Diego, CA, USA). Briefly, samples containing 200 μg of protein was loaded in one big well on top of a 4−15% gradient SDS-polyacrylamide gel and separated by electrophoresis (1.5 h at 150v). The proteins were transferred to Immobilon-FL membrane (Millipore, Billerica, MA, USA) for 2 h at 200 mA. After transfer, the membranes were incubated in the blocking buffer (LI-COR, Lincoln, NE, USA). The membrane was clamped with a Western blotting manifold that isolates 41 channels across the membrane. Each channel was incubated with a complex antibody cocktail for 1 h. The blots were removed from the manifold, washed, and hybridized for 30 min with secondary goat anti-mouse antibody conjugated to Alexa680 fluorescent dye (Molecular Probes, Eugene, OR, USA). Image data were captured using the Odyssey Infrared Imaging System (LI-COR). Data analysis included the raw and normalized signal intensity data from each blot. The results were expressed as fold change that represented the protein changes, either increasing or decreasing in the comparative analysis between the experimental samples and the control. The detected protein expression changes were listed in the order of confidence, 0 through 3, with 3 being the highest level of confidence, based on the signal quality. Only the data from confidence levels 2 and 3 (good quality signals; Supporting Information; Tables S1, S2a, S2b, and S2c) for proteins mapped to valid accessions were considered for further analysis. Proteins that displayed >1.8-fold change in abundance were judged to be differentially expressed, following the manufacturer's recommendation.

Human Orthologues for the Differentially Expressed Proteins

BD PowerBlot assay employs a cocktail of monoclonal antibodies that target human, mouse, and rat proteins, and in a specific study, over 90% were found to cross-react with proteins from human, mouse and rat[17] (Table S1). Human orthologues for the proteins picked up by the antibody cocktail were retrieved from KEGG (Tables S2a, S2b, and S2c).

Construction of Protein−Protein Interaction Networks

PPIs for the human orthologues of each set of differentially expressed proteins were retrieved from BioGRID 3.1.74[18] and iRefIndex 8.0[19] databases along with the interactions between the primary interactors of the differentially expressed proteins using TargetMine.[16] TargetMine is an integrated data warehouse that combines different biological data types and employs an objective protocol to prioritize candidate genes for further experimental investigation.[16] The interactions were merged and filtered for redundancy to infer overall extended PPI networks. Protein identifiers used in the different databases were mapped to Entrez gene IDs and official gene symbols. The official gene symbols are used hereafter, to refer to the differentially expressed proteins (Table 1) and their interacting partners. All the relationships discussed should be interpreted as protein relationships unless otherwise clarified.

PPI Network Topological Analysis

Network components were visualized using Cytoscape 2.6,[20] while network properties such as *node degree distribution* and *shortest path* measures were computed using the Cytoscape NetworkAnalyzer plugin[21] as described previously.[22] In a PPI network, the degree of a node (protein) is defined as the number of nodes directly connected to (interacting with) it, i.e., its first neighbors. *Node degree distribution*, $P(k)$, is the number of nodes with a degree k for k = 0, 1, 2, ... The *shortest path length* between two nodes n and m, $L(n,m)$, is the minimal number of interactions that link proteins n and m in a PPI network. The *shortest path length distribution* is the number of node pairs (n,m) with $L(n,m) = x$ for x = 1, 2, ... The *average shortest path length*, also known as the *characteristic path length*, gives the expected distance between two connected nodes i.e. the minimal number of interactions that link any two proteins in a PPI network.

Functional Analysis by Characterization of Enriched Biological Associations

Gene ontology (GO) associations retrieved from GO consortium,[23] biological pathway data from KEGG (retrieved on March 1, 2011),[24] and disease phenotype associations from OMIM[25] were used to assign functional annotations to the constituents of the extended PPI networks. The proteins in each of the extended PPI networks were uploaded to TargetMine to create protein lists, and the enrichment of specific biological themes (GO terms, KEGG Pathways, OMIM phenotypes) associated with each PPI network was estimated

dx.doi.org/10.1021/pr300121a | J. Proteome Res. 2012, 11, 3664−3679

Table 1. Summary of PowerBlot Detected Protein Expression Levels in Protein Samples

CoreTGvsWT

protein	gene ID	symbol	confidence level[a]	(−) under, (+) over[b]	fold change[c]
P31749	207	AKT1	3	−	2.68
P07355	302	ANXA2	3	+	2.92
O43747	164	AP1G1	3	+	5.72
P63010	163	AP2B1	3	+	2.40
Q96CW1	1173	AP2M1	2	+	1.93
Q9Y2T2	26985	AP3M1	2	+	1.89
P05089	383	ARG1	2	+	2.08
P52566	397	ARHGDIB	3	+	2.02
O15145	10094	ARPC3	2	−	2.25
P49407	408	ARRB1	3	−	2.33
Q07812	581	BAX	3	+	2.03
P55212	839	CASP6	3	−	1.95
Q14790	841	CASP8	2	+	2.18
Q03135	857	CAV1	2	+	2.07
P12830	999	CDH1	3	−	2.33
P19022	1000	CDH2	3	+	4.57
Q53SH4	1134	CHRNA1	3	−	3.11
P21964	1312	COMT	2	+	2.96
P00450	1356	CP	3	+	2.36
P21291	1465	CSRP1	3	+	2.23
P49711	10664	CTCF	3	+	6.13
P25685	3337	DNAJB1	3	−	2.16
P63241	1984	EIF5A	3	+	1.94
P42566	2060	EPS15	3	+	4.28
Q92889	2072	ERCC4	3	+	5.43
O75899	9568	GABBR2	3	+	3.39
O43719	27336	HTATSF1	3	+	5.76
P06756	3685	ITGAV	3	+	6.32
Q14974	3837	KPNB1	3	−	1.86
Q16539	1432	MAPK14	3	−	2.81
Q9UPY8	22924	MAPRE3	3	+	2.46
P49736	4171	MCM2	3	+	1.87
P62166	23413	NCS1	3	−	2.24
Q8IZS7	140767	NRSN1	3	+	1.89
Q16620	4915	NTRK2	3	+	2.40
Q14980	4926	NUMA1	3	−	1.94
P07237	5034	P4HB	3	+	2.27
Q92878	10111	RAD50	3	+	4.93
Q99638	5883	RAD9A	2	−	3.10
P20936	5921	RASA1	3	+	1.86
Q96SB4	6732	SRPK1	3	+	3.11
Q92186	8128	ST8SIA2	3	+	5.11
P42224	6772	STAT1	3	+	2.00
P40763	6774	STAT3	3	+	2.30
Q9UNK0	9482	STX8	3	+	1.88
Q12800	7024	TFCP2	3	+	5.04
Q92752	7143	TNR	3	+	5.36
Q13263	10155	TRIM28	3	+	4.70
O43396	9352	TXNL1	3	−	4.82
P50552	7408	VASP	2	−	2.61
Q96AJ9	143187	VTI1A	3	+	3.25
Q14191	7486	WRN	3	+	17.12

altered protein levels in PA28$\gamma^{-/-}$CoreTGvsWT

protein	gene ID	symbol	confidence level[a]	(−) under, (+) over[b]	fold change[c]
O15145	10094	ARPC3	2	−	1.96
P49407	408	ARRB1	3	−	2.17
P55212	839	CASP6	3	−	2.04

altered protein levels in PA28$\gamma^{-/-}$CoreTGvsWT

protein	gene ID	symbol	confidence level[a]	(−) under, (+) over[b]	fold change[c]
O60508	51362	CDC40	2	+	1.99
P54105	1207	CLNS1A	3	+	2.41
P21964	1312	COMT	2	+	2.71
P67870	1460	CSNK2B	3	+	1.90
P78352	1742	DLG4	2	+	4.08
Q95GK7	1837	DTNA	3	−	2.42
P55010	1983	EIF5	3	+	2.19
Q08495	2039	EPB49	3	+	2.66
P37268	2222	FDFT1	2	+	5.68
P09038	2247	FGF2	2	+	2.69
P62962	2280	FKBP1A	2	+	1.89
O75146	9026	HIP1R	2	−	2.08
Q9NZL4	23640	HSPBP1	3	+	3.46
P05412	3725	JUN	2	+	2.15
P52292	3838	KPNA2	3	−	7.28
P36507	5605	MAP2K2	3	−	2.35
Q16539	1432	MAPK14	3	−	3.29
P22033	4594	MUT	3	+	2.46
P54920	8775	NAPA	2	−	1.97
Q8IZS7	140767	NRSN1	3	+	1.93
Q16620	4915	NTRK2	3	+	2.50
P07237	5034	P4HB	3	+	2.04
Q08209	5530	PPP3CA	3	+	7.55
Q06124	5781	PTPN11	2	+	2.33
Q99638	5883	RAD9A	2	−	1.97
P43487	5902	RANBP1	3	+	2.29
Q9UPX8	22941	SHANK2	3	−	1.94
P29353	6464	SHC1	3	+	3.27
Q92186	8128	ST8SIA2	3	+	4.06
P31948	10963	STIP1	3	−	1.99
O75558	8676	STX11	2	+	2.04
P23193	6917	TCEA1	3	−	2.17
P07101	7054	TH	2	+	2.78
P13693	7178	TPT1	3	−	1.93
Q15628	8717	TRADD	3	−	2.00
P50607	7275	TUB	3	+	1.91

altered protein levels in PA28$\gamma^{-/-}$CoreTGvsCoreTG

protein	gene ID	symbol	confidence level[a]	(−) under, (+) over[b]	fold change[c]
P07355	302	ANXA2	3	−	2.96
O43747	164	AP1G1	3	−	4.20
P63010	163	AP2B1	3	−	3.01
Q96CW1	1173	AP2M1	2	−	1.88
Q9Y2T2	26985	AP3M1	3	+	2.38
O00499	274	BIN1	2	−	1.88
Q9UQM7	815	CAM2KA	3	+	2.06
Q8N5S9	84254	CAMKK1	2	+	5.78
P19022	1000	CDH2	3	−	3.85
P25108	1134	CHRNA1	3	+	2.55
P49674	1454	CSNK1E	3	+	1.97
P67870	1460	CSNK2B	3	+	1.88
P21291	1465	CSRP1	3	+	1.87
P49711	10664	CTCF	3	−	5.43
Q8WTW3	9382	COG1	3	−	7.02
P00450	1356	CP	3	−	3.55
Q13618	8452	CUL3	3	+	1.91
P78352	1742	DLG4	2	+	2.13
Q9Y4J8	1837	DTNA	3	−	2.94

dx.doi.org/10.1021/pr300121a | J. Proteome Res. 2012, 11, 3664−3679

Table 1. continued

altered protein levels in PA28γ⁻/⁻CoreTGvsCoreTG					
protein	gene ID	symbol	confidence level[a]	(−) under, (+) over[b]	fold change[c]
Q08495	2039	EBP49	3	+	2.30
O14682	8507	ENC1	3	+	2.88
P42566	2060	EPS15	3	−	2.11
Q92889	2072	ERCC4	3	−	3.49
P09038	2247	FGF2	2	−	2.18
P62962	2280	FKBP1A	2	+	2.59
P49356	2342	FNTB	2	+	1.95
O75899	9568	GABBR2	3	−	2.53
O75146	9026	HIP1R	3	−	1.97
Q9NZL4	23640	HSPBP1	3	+	3.60
P61604	3336	HSPE1	3	−	2.17
Q99730	27336	HTATSF1	3	−	9.24
Q9Y6K9	8517	IKBKG	2	+	1.97
P52292	3838	KPNA2	3	−	3.94
P36507	5605	MAP2K2	3	−	2.66
Q13505	4580	MTX1	3	−	1.90
P62166	23413	NCS1	3	+	2.56
Q14980	4926	NUMA1	2	+	1.87
P41236	5504	PPP1R2	3	−	2.25
Q08209	5530	PPP3CA	3	+	12.94
P13861	5576	PRKAR2A	3	−	1.88
Q15276	9135	RABEP1	2	−	2.74

altered protein levels in PA28γ⁻/⁻CoreTGvsCoreTG					
protein	gene ID	symbol	confidence level[a]	(−) under, (+) over[b]	fold change[c]
Q92878	10111	RAD50	3	−	5.19
P20936	5921	RASA1	3	+	2.50
P06400	5925	RB1	3	+	2.50
Q92854	10507	SEMA4D	2	+	2.00
Q92529	53358	SHC3	3	−	1.90
P63208	6500	SKP1	3	−	2.45
P43004	6506	SLC1A2	2	+	2.27
Q4U2R8	9356	SLC22A6	3	−	2.23
P42224	6772	STAT1	3	−	1.90
P31948	10963	STIP1	3	−	1.98
O75558	8676	STX11	2	+	3.52
Q8IZU3	50511	SYCP3	3	+	1.88
P07101	7054	TH	2	+	2.62
Q92752	7143	TNR	3	−	4.62
O43396	9352	TXNL1	2	+	3.05
P13693	7178	TPT1	3	−	2.85
Q13263	10155	TRIM28	3	−	3.53
Q15628	8717	TRADD	3	−	2.98
P50607	7275	TUB	3	+	1.96
P41542	8615	USO1	3	−	2.05
Q14191	7486	WRN	3	−	3.44

[a]Defined as follows: Level 3 = changes greater than 2-fold from good quality signals that also pass a visual inspection. Level 2 = changes greater than 2-fold from good quality signals that do not pass a visual inspection. [b]+ indicates an increase in protein level in the experimental sample relative to control. − indicates a decrease in protein level in the experimental sample relative to control. [c]A semiquantitative value that represents the general trend of protein changes for the experimental sample relative to control.

by performing the hypergeometric test within TargetMine.[16] The inferred p-values were further adjusted for multiple test correction to control the false discovery rate using the Benjamini and Hochberg procedure,[26,27] and the annotations/pathways were considered significant if $p \leq 0.05$.

Transcription Factor-Target Associations

Transcription factor (TF)-target associations for the differentially expressed proteins were retrieved from the TF-target repository compiled from Amadeus[28] and ORegAnno[29] in TargetMine[16] and are discussed in the Supporting Information.

RNAi and Transfection

The siRNA pair targets to VTI1A, STX8, and COMT were purchased from Ambion (Ambion, Austin, TX, USA). Stealth RNAi Negative Control Low GC Duplex (Invitrogen, Carlsbad, CA, USA) was used as a control siRNA. Each siRNA duplex was introduced into the cell lines by using lipofectamine RNAiMax (Invitrogen). Ambion ID numbers of siRNA duplex of VTI1A and STX8 were S225671 and S18183, respectively. The replicon cell line, as will be described below, was transfected with each siRNA at a final concentration of 20 nM as per the manufacturer's protocol and then seeded at 2.5×10^4 cells per well of a 24-well plate. The transfected cells were harvested at 72 h post-transfection. The Huh7OK1 cell line, as will be described below, was transfected with each siRNA at a final concentration of 20 nM as per the manufacturer's protocol and then seeded at 2.5×10^4 cells per well of a 24-well plate. The transfected cells were infected with JFH1 at an MOI of 0.05 at 24 h post-transfection. The resulting cells were harvested at the indicated time.

Quantitative Reverse-Transcription PCR (qRT-PCR)

Total RNA was prepared from the cell and culture supernatant using the RNeasy mini kit (QIAGEN, Hilden, Germany) and QIAamp Viral RNA Mini Kit (QIAGEN), respectively. First-strand cDNA was synthesized using a high capacity cDNA reverse transcription kit (Applied Biosystems, Carlsbad, CA, USA) with random primers. Each cDNA was estimated by Platinum SYBR Green qPCR Super Mix UDG (Invitrogen) as per the manufacturer's protocol. Fluorescent signals of SYBR Green were analyzed with ABI PRISM 7000 (Applied Biosystems). The HCV internal ribosomal entry site (IRES) region and human glyceraldehyde-3-phosphate dehydrogenase (GAPDH) gene were amplified with the primer pairs 5′-GAGTGTCGTGCAGCCTCCA-3′ and 5′-CACTCGCAAGCACCCTATCA-3′, and 5′-GAAGGTCGGAGTCAACGGATT-3′ and 5′-TGATGACAAGCTTCCCGTTCTC-3′, respectively.[30] The quantities of the HCV genome and the other host mRNAs were normalized with that of GAPDH mRNA. VTI1A and STX8 genes were amplified using the primer pairs 5′-TGACAGGGATGTTGCGAAGA-3′ and 5′-CAACCCACATGCAAACAGGA-3′, and 5′-TTGAAGGGGACCGAAGACAGAACCTC-3′, and 5′-TCAAAACCCAAGCCTCTGGTCTCCT-3′, respectively.

Cell Lines and Virus Infection

Cells from the Huh7OK1 cell line are highly permissive to HCV JFH1 strain (genotype 2a) infection compared to Huh 7.5.1 and exhibit the highest propagation efficiency for JFH1.[30] These cells were maintained at 37 °C in a humidified atmosphere and 5% CO_2, in Dulbecco's modified Eagle's medium (DMEM) (Sigma, St. Louis, MO, USA) supplemented with nonessential amino acids (NEAA), sodium pyruvate, and

dx.doi.org/10.1021/pr300121a | J. Proteome Res. 2012, 11, 3664−3679

10% fetal calf serum (FCS). The human hepatoma cell line Huh7, harboring the full genome of the HCV Con1 strain (genotype 1b), was prepared as described by Pietschmann et al.[31] We also established an Huh7 cell line harboring the subgenome of the JFH1 strain by the transfection of the plasmid pSGR-JFH1.[32] The Huh7-derived cell lines harboring a full length HCV replicon were maintained in DMEM containing 10% FCS, nonessential amino acids, sodium pyruvate, and 1 mg/mL G418 (Nakarai Tesque, Tokyo, Japan). The viral RNA of JFH1 was introduced into Huh7OK1 as described by Wakita et al.[33] The viral RNA of JFH1 derived from the plasmid pJFH1 was prepared as described by Wakita et al.[33]

Statistical Analysis

Experiments for RNAi transfection and qRT-PCR were performed three times. The estimated values were represented as the mean ± standard deviation (n = 3). The significance of differences in the means was determined by the Student's t test.

RESULTS AND DISCUSSION

Core Expression and PA28γ Knockout Induce Substantial Changes in the Expression Levels of Host Proteins Associated with HCV Infection in the Liver

The PowerBlot immunoblots showed proteins with increased or decreased levels (defined as those that displayed >1.8-fold change in abundance) in the transgenic samples relative to the WT samples and also relative to each other. In all, we identified 37 proteins with increased levels and 15 proteins with decreased levels in CoreTGvsWT, 24 proteins with increased levels and 15 proteins with decreased levels in PA28$\gamma^{-/-}$-CoreTGvsWT, and 26 proteins with increased levels and 36 proteins with decreased levels in PA28$\gamma^{-/-}$CoreTGvsCoreTG. While most proteins with altered abundance display changes between 1.8-fold and 6-fold, some proteins displayed much higher fold changes. For instance, WRN protein levels increased 17-fold in CoreTGvsWT (Table 1).

Our analysis detected changes in the abundance of proteins, known to be associated with HCV pathogenesis, in the liver samples from CoreTG compared with WT. These include Arginase I (ARG1; +2.08-fold), a liver enzyme associated with the polyamine metabolism, which is known to be overexpressed in HCV-mediated hepatocarcinogenesis;[34] STAT3 (+2.30-fold), which is directly activated by the Core and HCV-mediated oxidative stress facilitating tumorigenesis and is also essential for HCV replication;[35−37] STAT1 (+2-fold), which interacts with Core and facilitates the HCV-mediated attenuation of the host interferon signaling;[38] and MAPK14 (p38 MAPK; −2.81-fold), which is cooperatively activated by Core and ethanol in HCV infection[39] (Table 1). These results are in line with the previous observations that Core expression can induce HCV pathogenesis and hepatocarcinogenesis in transgenic mice.[2] Among other examples, BIN1, which interacts with the HCV NS5A protein and contributes to the pathogenesis of HCC,[40] was suppressed 1.88-fold in PA28$\gamma^{-/-}$CoreTGvsCoreTG; this is consistent with the lack of HCC pathogenesis in PA28$\gamma^{-/-}$CoreTG mice. Similar studies have aimed to characterize the global changes in the host transcriptome and proteome in response to HCV infection.[41−44] These studies, however, have not provided specific insights into PA28γ's roles in HCV pathogenesis. Our observations suggest that the PowerBlot assay was able to capture successfully some of the molecular signatures associated with the Core-PA28γ interplay in HCV pathogenesis.

Topological Analysis of the Extended Protein Interaction Networks

To further understand the biological significance of the differential protein levels, we retrieved PPIs for the proteins with increased and decreased levels in CoreTGvsWT, PA28$\gamma^{-/-}$CoreTGvsWT, and PA28$\gamma^{-/-}$CoreTGvsCoreTG and inferred the corresponding extended protein interaction networks for each data set using TargetMine (see Materials and Methods). First, we computed the *node degree distribution* and *characteristic/average path length* measures to capture the topology of the extended PPI networks as described earlier.[22] The degree of a protein, which corresponds to the number of its interacting partners, may often reflect its biological relevance since a better connected protein may have a higher ability of influencing biological networks via PPIs. Average path lengths provide an approximate measure of the relative ease and speed of transfer of information between the proteins in a network. The CoreTGvsWT extended network was made up of 1373 entities (proteins) with 12535 interactions, the PA28$\gamma^{-/-}$CoreTGvsWT extended network of 1057 entities with 8988 interactions, and the PA28$\gamma^{-/-}$CoreTGvsCoreTG of 1476 entities with 12871 interactions between them, respectively (Tables S3, S4). For comparison, we also derived an extended PPI network for all the non-genetic PPIs in the human genome as compiled in BioGRID and iRefindex repositories (data not shown). The average degree (defined as the number of interactions for a given protein) of the CoreTGvsWT (17.31), PA28$\gamma^{-/-}$CoreTGvsWT (16.1), and PA28$\gamma^{-/-}$CoreTGvsCoreTG (16.57) extended networks was higher than the degree inferred for the human interactome (10.17). This observation suggests that HCV infection targets several highly connected cellular proteins with an ability to influence a large number of host factors in HCV pathogenesis. The average (shortest) path lengths of the three extended networks (2.93, 2.9, and 2.97, respectively) were significantly shorter than that inferred for the human interactome (3.88), suggesting that the Core and PA28γ influenced cellular networks are more compact and inclined toward faster communication between the constituents relative to the human interactome (Figure 1). Our observations are consistent with previous studies on the protein interaction networks associated with HCV infection.[22,45]

The compactness of the HCV-influenced protein networks coupled with the ability to influence a wide array of factors in the host cellular networks may facilitate a rapid propagation of the signaling information and allow the virus to respond rapidly to the host mobilization against HCV infection.

Functional Analysis of the Extended Protein Interaction Networks

Next, we investigated the extended networks for the enrichment of specific biological associations (KEGG pathways, GO terms, and OMIM phenotypes, Tables S5, S6, and S7). The analysis of the CoreTGvsWT, PA28$\gamma^{-/-}$CoreTGvsWT, and PA28$\gamma^{-/-}$CoreTGvsCoreTG extended networks revealed an enrichment ($p \leq 0.05$) of 116, 104, and 118 KEGG pathways, respectively (Table S5). Below we describe our observations on the selected enriched biological themes of interest, chiefly associated with the PA28$\gamma^{-/-}$CoreTGvsCoreTG network. Functional associations for the host factors previously known to be associated with HCV pathogenesis and HCC are

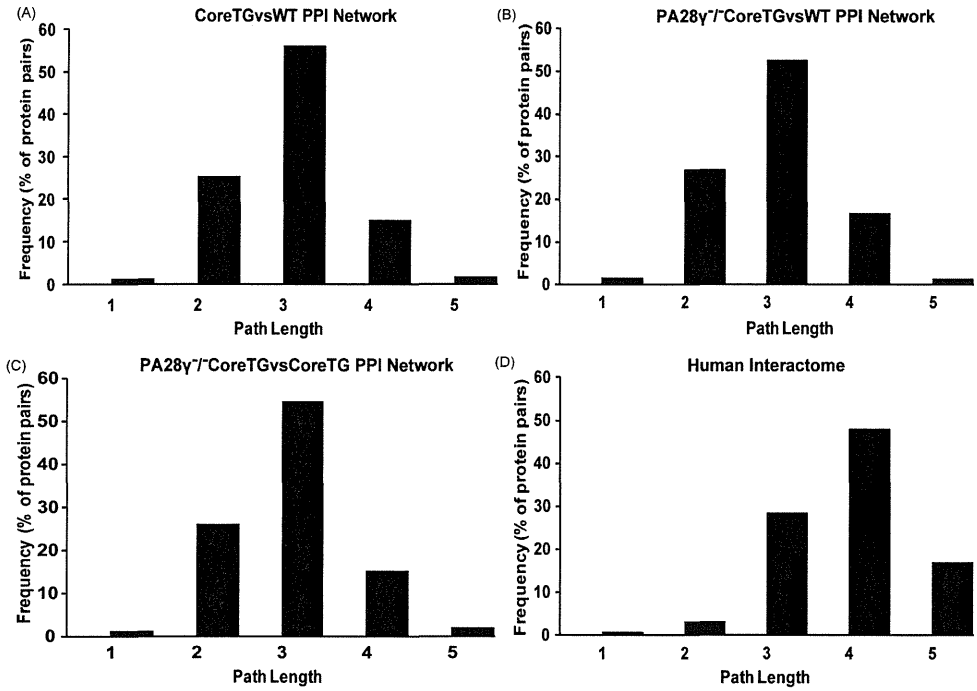

Figure 1. Graphical representation of the shortest path length distribution for (A) CoreTGvsWT extended network, (B) PA28$\gamma^{-/-}$CoreTGvsWT extended network, (C) PA28$\gamma^{-/-}$CoreTGvsCoreTG extended network, and (D) human protein interactome. The path length is represented on the x-axis, while the y-axis describes the frequency, i.e., the percentage of node (protein) pairs within the PPI network with a given shortest path length. For simplicity, only the node frequencies for path lengths 1–5 are displayed.

summarized in Table 2. Specific functional associations for the CoreTGvsWT and PA28$\gamma^{-/-}$CoreTGvsWT networks, except when discussed below, are detailed in the Supporting Information. It will highlight the biological significance of the differentially expressed proteins, their interactions, and their probable roles in HCV infection and help identify potentially novel regulators of and biomarkers for HCV pathogenesis.

Vesicular Transport

HCV infection involves the formation of the HCV replication complex in the detergent-resistant membrane (DRM) fraction or lipid rafts. These subcellular membrane fractions are utilized by some pathogens including viruses to facilitate viral entry and assembly.[46−49] HCV infection induces modifications in the host lipid raft proteome, which directly impacts HCV replication in the infected cells.[50] Core targeting to the early and late endosomes and the viral particle production requires the components of the endosome-based secretory pathways.[51,52]

CoreTGvsWT Extended Network. The PowerBlot analysis revealed the two endosomal proteins VTI1A and STX8 (KEGG Pathway "SNARE interactions in vesicular transport"; p = 0.023; Table S5) that were upregulated 3.25- and 1.88-fold, respectively, in CoreTGvsWT (Table 1). SNAREs are membrane-anchored proteins involved in membrane trafficking.[53] Some SNAREs may function in HCV egress by possibly facilitating the fusion of the late endosomes that carry HCV particles with the plasma membrane resulting in their release into the extracellular environment.[52] VTI1A is a SNARE involved in the vesicular transport from the late endosomes to the trans-Golgi network and forms a SNARE complex with STX16 and VAMP4 (Table S4).[54,55] STX8 is involved in the protein trafficking from the early to the late endosomes and exocytosis and forms a SNARE complex with STX7, VAMP8, and VTI1B.[55,56] A reduction in the expression of STX7, which interacts with both VTI1A and STX8 (Figure 2; Table S4), decreases HCV replication.[50] Taken together, the increased abundances of VTI1A and STX8 in CoreTGvsWT, but not PA28$\gamma^{-/-}$CoreTGvsWT, suggest potentially crucial roles of the two proteins in the HCV life cycle.

PA28$\gamma^{-/-}$CoreTGvsCoreTG Extended Network. Syntaxin 11 (STX11), a SNARE, was upregulated 3.52-fold in PA28$\gamma^{-/-}$CoreTGvsCoreTG (Table 1) and was mapped to the enriched KEGG Pathway "SNARE interactions in vesicular transport" (p = 0.003; Table S5). STX11 associates with the late endosomes and functions in the essential trafficking pathways (such as cytokine secretion) in the immune cells, with enhanced STX11 expression contributing to increased NK-cell mediated cytotoxicity.[57−61] STX11 binds with the SNARE VTI1B (Figure 3, Table S4) and regulates its participation the Q-SNARE complexes and, thus, the endocytic and exocytic trafficking in the macrophages. Overexpression of STX11 alters the VTI1B binding to STX6 and STX8 and likely reduces the endosomal transport to the cell surface.[57]

USO1, a Golgi-associated peripheral membrane protein, was decreased 2.05-fold in PA28$\gamma^{-/-}$CoreTGvsCoreTG (Table 1) and was identified as a significant linking component of the PA28$\gamma^{-/-}$CoreTGvsCoreTG SNARE network (Figure 3). USO1 plays an important role in ER to Golgi trafficking and its knockdown leads to the disintegration of the Golgi complex.[62,63] Decreased USO1 levels in PA28$\gamma^{-/-}$CoreTGvsCoreTG may, therefore, significantly impact the endosomal pathways associated with HCV release.

PA28γ knockdown impairs the production of the infectious HCV particles (but not replication) in the JFH1 (HCV genotype 2a) infected cells, largely due to the deregulation of the E6AP-dependent Core degradation, which contributes to an antiviral response.[14] Our analysis suggests a potentially novel

dx.doi.org/10.1021/pr300121a | J. Proteome Res. 2012, 11, 3664–3679

Table 2. Functional Analysis of the Extended Protein Interaction Networks[a]

proteins	data set[b]	KEGG pathways	prior involvement with HCV pathogenesis and HCC	probable associations with Core/PA28γ functions in HCV pathogenesis
AKT1	I (−)	Insulin signaling pathway ($p = 5.72 \times 10^{-12}$)	reduced levels associated with insulin resistance (IR) in rats;[105] Akt phosphorylation is suppressed in the CoreTG mice and contributes to IR.[12]	Core-induced suppression of AKT1 levels may contribute to IR in HCV pathogenesis.
BAX	I (+)	Apoptosis ($p = 1.58 \times 10^{-18}$)	interacts with NS5A; disrupts mitochondrial homeostasis leading to abnormal cytochrome *c* release and apoptosis in HCV infection.[45,90,92,93]	Core-mediated BAX upregulation may induce host cell apoptosis.
CASP8	I (+)	Apoptosis ($p = 1.58 \times 10^{-18}$)	activated in HCV infection.[90]	Core-mediated CASP8 upregulation may induce host cell apoptosis.
CDH1	I (+)	Adherens junction ($p = 1.45 \times 10^{-20}$)	downregulated in the rat liver during hepatocarcinogenesis[106]	Core-mediated decrease in CDH1 levels may contribute to HCC
COMT	I (+); II (+)	Steroid hormone biosynthesis ($p = 0.002$)	upregulated in the lipid rafts in HCV infection;[50] COMT siRNA knockdown decreases HCV replication[103]	Core-induced activation of COMT may play an important role in HCV entry and replication
CSNK2B	II (+); III (+)	Adherens junction ($p = 1.4 \times 10^{-13}$); tight junction ($p = 4.46 \times 10^{-7}$)	interacts with the HCV NS3 protein;[45] regulates NS5A phosphorylation and hence infectious HCV particle production.[87]	loss of PA28γ activity may perturb CK2-mediated NS5A phosphorylation leading to decreased viral propagation.
EPS15	I (+); III (−)	Endocytosis ($p = 2.08 \times 10^{-22}$)	elevated in human and mouse HCC;[107] mediates human enterovirus 71 entry via clathrin-mediated endocytosis,[108] which also mediates HCV internalization.[109]	elevated EPS15 levels may facilitate HCC; decreased EPS15 levels may contribute to the lack of HCC in the PA28$\gamma^{-/-}$CoreTG. May facilitate HCV entry via clathrin-mediated endocytosis.
MCM2	I (+)	Cell cycle ($p = 1.82 \times 10^{-25}$)	increased hepatocyte MCM2 expression linked with fibrosis progression in HCV infection.[110]	Core-mediated enhanced MCM2 activity may contribute to fibrosis in HCV pathogenesis.
PTPN11	II (+)	Natural killer cell mediated cytotoxicity ($p = 3.64 \times 10^{-10}$); Jak-STAT signaling pathway ($p = 5.74 \times 10^{-5}$)	functions as a tumor suppressor in HCC and negatively regulates hepatic insulin action.[111,112]	increased PTPN11 levels may be associated with the absence of HCC progression in PA28$\gamma^{-/-}$CoreTG.
RABEP1	III (−)	Endocytosis ($p = 2.08 \times 10^{-22}$)	interacts with NS3;[45] functions in early endocytic events and regulates mast cell activation.[113,114]	may possibly function in HCV propagation.
RB1	III (+)	Cell cycle ($p = 4.04 \times 10^{-20}$)	tumour suppressor, downregulated in HCC.[115,116]	increased RB1 levels in III consistent with the lack of HCC progression in the PA28$\gamma^{-/-}$CoreTG mice.
TRADD	III (−)	Apoptosis ($p = 1.84 \times 10^{-15}$)	forms a complex with Core and TNFR1, implicated in HCV-induced chronic liver disease.[117]	decreased TRADD levels may contribute to the lack of IR and liver disease in PA28$\gamma^{-/-}$CoreTG

[a]Host factors that were previously known to be associated with HCV pathogenesis and HCC and were mapped to various enriched KEGG pathways associated with the CoreTGvsWT, PA28$\gamma^{-/-}$CoreTGvsWT, and PA28$\gamma^{-/-}$CoreTGvsCoreTG PPI networks. [b]Data set I: CoreTGvsWT; Data set II: PA28$\gamma^{-/-}$/CoreTGvsWT; Data set III: PA28$\gamma^{-/-}$/CoreTGvsCoreTG; +: upregulated; −: downregulated.

dx.doi.org/10.1021/pr300121a | J. Proteome Res. 2012, 11, 3664−3679

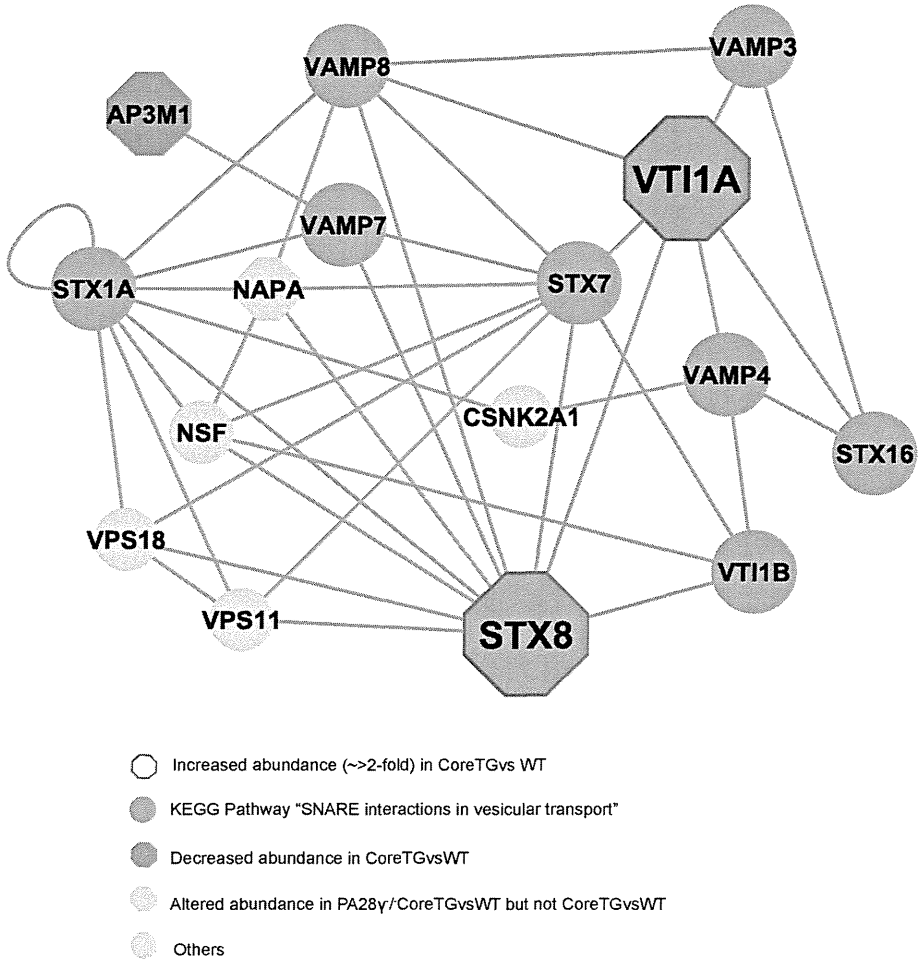

Figure 2. CoreTGvsWT SNARE network. Network illustration of the interactions between the PowerBlot identified differentially expressed proteins in CoreTGvsWT and human proteins mapped to the enriched KEGG pathway "SNARE interactions in vesicular transport". The node sizes differ for better clarity and do not reflect any topological attributes.

mechanism for the involvement of PA28γ in HCV propagation. Potentially, the suppression of PA28γ activity in PA28$\gamma^{-/-}$CoreTG mice may contribute to the overexpression of STX11 (and downregulation of USO1), thereby impairing the trafficking to the cell surface and consequently the release of the infectious HCV particles.

HCV has also been detected in the macrophages of certain infected patients,[64] suggesting that HCV may possibly infect the macrophages *in vivo* and regulate the STX11 (and USO1) expression to modulate the viral release and cytokine secretion.

EPS15 and RABEP1 (KEGG pathway "Endocytosis", $p = 2.08 \times 10^{-22}$) were decreased 2.11- and 2.74-fold, respectively, in PA28$\gamma^{-/-}$CoreTGvsCoreTG (Table 1, Table S5). EPS15 is an adaptor protein associated with the epidermal growth factor (EGF) signaling; it is localized to the clathrin-coated pits and functions in receptor-mediated endocytosis[65,66] and may play an important role in HCV pathogenesis (Table 2).

Immune System and Signal Transduction

HCV infection induces varied active and passive host immune responses such as the recognition of the infecting HCV RNA and proteins by the macrophages and the dendritic cells expressing Toll-like receptors (TLRs) and RIG-I-like receptors (RLRs). These events trigger the production of Type I interferons (IFN-α/β) and inflammatory cytokines in the infected hepatocytes, thereby initiating viral clearance. The ability to impair host immune responses contributes to the HCV persistence in the host.[67−72]

The PowerBlot analysis showed differentially expressed host proteins (IKBKG, MAP2K2, PPP3CA, SHC3, STAT1, TRADD) in PA28$\gamma^{-/-}$CoreTGvsCoreTG and their interacting partners that were mapped to one or more enriched KEGG pathways associated with the immune system (Table S5). IKBKG (IKK Gamma) is an antiapoptotic protein that is essential for NFKB activation and modulates TNF-mediated apoptosis.[73] IKBKG mutations are associated with immune deficiency phenotype (Table S7) and IKBKG may contribute to the activity of the hepatic carcinoma associated protein MAFIP in suppressing the proliferation of the cancer cells.[74] Additionally, specific deletion of IKBKG in the hepatocytes promotes NK-cell dependent liver damage.[75] Taken together, the elevated IKBKG abundance as observed in PA28$\gamma^{-/-}$CoreTGvsCoreTG (1.97-fold; Table 1) may contribute to the lack of HCC progression and reduced liver damage in the PA28$\gamma^{-/-}$CoreTG mice.

PPP3CA, MAP2K2, and SHC3 were mapped to the KEGG pathway "Natural killer cell mediated cytotoxicity" ($p = 1.67 \times 10^{-5}$; Table S5), the components of which function in the host immune response against the cancer cells and cells beset with pathogen infection.[76] PPP3CA levels were increased 12.94-fold,

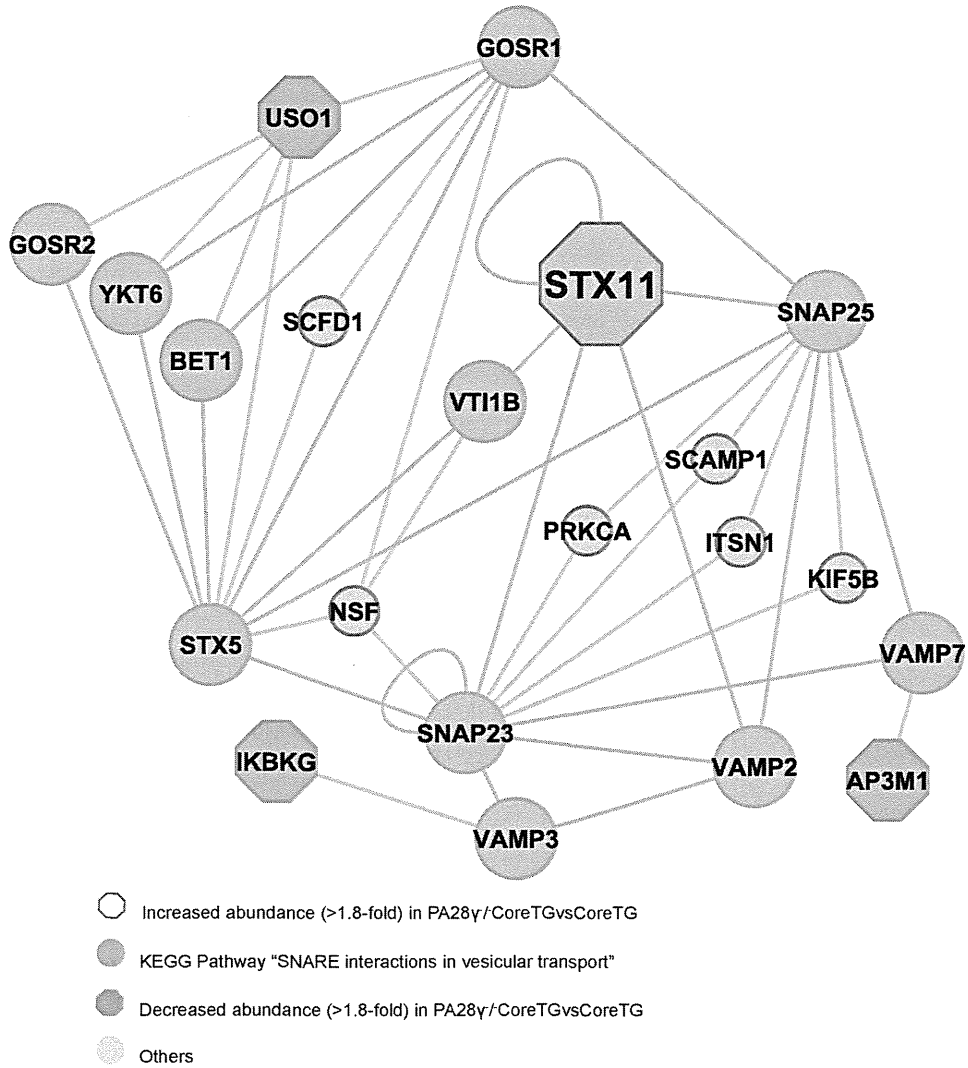

Figure 3. PA28$\gamma^{-}/^{-}$CoreTGvsCoreTG SNARE network. Network illustration of the interactions between the PowerBlot identified differentially expressed proteins in PA28$\gamma^{-}/^{-}$CoreTGvsCoreTG and human proteins mapped to the enriched KEGG pathway "SNARE interactions in vesicular transport". The node sizes differ for better clarity and do not reflect any topological attributes.

while MAP2K2 and SHC3 levels were suppressed 2.35-fold and 1.9-fold, respectively, in PA28$\gamma^{-/-}$CoreTGvsCoreTG (Table 1). These observations together with the increased STX11 abundance are consistent with the enhanced NK-cell mediated cytotoxicity that accompanies the STX11 overexpression.

PPP3CA is a tumor suppressor that negatively modulates the vascular endothelial growth factor (VEGF)-stimulated cell proliferation[77] and is downregulated in some cancerous cells.[78,79] PPP3CA was also mapped to the enriched KEGG pathways "VEGF signaling pathway" ($p = 2.59 \times 10^{-5}$), "MAPK signaling pathway" ($p = 2.37 \times 10^{-16}$) and "Wnt signaling pathway" ($p = 1.048 \times 10^{-10}$; Table S5), which are implicated in the HCV infection and HCC. The 7.55-fold increase in PPP3CA abundance in PA28$\gamma^{-/-}$CoreTGvsCoreTG (Table 1) suggests that increased PPP3CA activity may significantly contribute to the lack of tumorigenesis and HCC progression in PA28$\gamma^{-/-}$CoreTG mice.

MAP2PK2 is a dual specificity MAP kinase that plays a critical role in the mitogen growth factor signal transduction. It is a key regulator of the TNF-α signaling and plays an important role in the tumor progression in certain cancers.[80] Reduced MAP2K2 levels in the hepatocytes are implicated in enhanced apoptosis.[81] Therefore, the 2.66-fold decrease in MAP2K2 protein levels in PA28$\gamma^{-/-}$CoreTGvsCoreTG (Table 1) suggests that decreased MAP2K2 activity may contribute to the lack of HCC progression in PA28$\gamma^{-/-}$CoreTG mice. Our analysis thus identified potentially significant PA28γ-dependent roles of MAP2K2 and PPP3CA in a probable STX11-mediated regulation of NK cell activity in HCV pathogenesis.

MAP2K2, PPP3CA and SHC3 were also associated with the "Insulin signaling pathway" ($p = 5.88 \times 10^{-9}$; Table S5), the disruption of which may contribute to insulin resistance (IR). IR is linked with steatosis, fibrosis progression and poor interferon-α response in HCV infection.[82,83] PA28γ contributes to hyperinsulinemia and IR in the CoreTG mice by impairing the insulin-signaling pathway through the suppression of Insulin receptor substrate 1 (IRS1) phosphorylation and increased tumor necrosis factor alpha (TNF-α) secretion.[12,84] The Powerblot analysis revealed that TRADD, which regulates TNF-α signaling as an antiapoptotic factor[85,86] and possibly functions in HCV pathogenesis (Table 2), was suppressed 2-fold in PA28$\gamma^{-/-}$CoreTGvsWT (Table 1).

dx.doi.org/10.1021/pr300121a | J. Proteome Res. 2012, 11, 3664–3679

Table 3. Summary of Proteins and Pathways Prioritized with TargetMine and Adjusted with the Help of Knowledge-Based Inputs for Experimental Investigation and/or Biomarker Discovery

(a) HCV replication and release

KEGG pathways	*p*-value	proteins[a]	data set[b]	knowledge-based evidence	refs
SNARE interactions in vesicular transport	0.023	VTI1A (+), STX8 (+)	I	regulation of the endosome-based membrane trafficking pathway implicated in HCV release	50, 52, 55
Steroid hormone biosynthesis	0.002	COMT (+)	I	COMT siRNA impairs HCV genotype 1b replication; functions in genotype 2a replication not known	50, 103
SNARE interactions in vesicular transport	0.003	STX11 (+)	III	modulation of specific components of the endosome-based membrane trafficking pathway implicated in HCV release; modulation of cytokine secretion in immune cells	50, 55, 57
Endocytosis	1.03×10^{-18}	CAV1 (+)	I	close homologue CAV2 associated with HCV replication complex; possible role in HCV replication	103

(b) steatosis, fibrosis, and hepatcarcinogenesis in HCV infection

KEGG pathways	*p*-value	proteins[a]	data set[b]	knowledge-based evidence	refs
Insulin signaling pathway	5.72×10^{-12}	AKT1 (−)	I	reduced AKT1 levels and phosophorylation associated with insulin resistance, which contributes to steatosis, fibrosis and HCC	118
Natural killer cell mediated cytotoxicity	1.67×10^{-5}	PPP3CA (+), MAP2K2 (−)	III	PPP3CA is a tumor suppressor with decreased levels in some cancers; PTPN1 is a tumor suppressor and regulates hepatic insulin signaling; decreased MAP2K2 levels in hepatocytes associated with enhanced apoptosis	78, 79, 81
Adherens junction	1.45×10^{-20}	CDH1 (−)	I	decreased CDH1 abundance associated with hepatocarcinogenesis and various cancers	106
Focal adhesion	5.57×10^{-12}	SHC1 (+)	II	loss of SHC1 function associated with tumor metastasis	119
Apoptosis	1.58×10^{-18}	BAX (+), CASP8 (+)	I	BAX interacts with NS5A and contributes to abnormal cytochrome *c* release in HCV infection; CASP8 activated in HCV infection	45, 90, 92, 93
Apoptosis	1.84×10^{-15}	TRADD (−)	III	antiapoptotic factor that forms a ternary complex containing Core, with likely functions in HCV-induced chronic liver disease	117
Chemokine signaling pathway	1.18×10^{-13}	ARRB1 (−)	I	interacts with PKM2, a key enzyme in glycolytic metabolism and cell growth and death in tumor cells	120

[a]+: upregulated. −: downregulated. [b]Data set I: CoreTGvsWT; Data set II: PA28$\gamma^{-/-}$/CoreTGvsWT; Data set III: PA28$\gamma^{-/-}$/CoreTGvsCoreTG.

Cell Adhesion

The Powerblot analysis revealed that host protein CSNK2B, the regulatory (beta) subunit of Casein Kinase II (CK2), was increased 1.88-fold in PA28$\gamma^{-/-}$CoreTGvsCoreTG (1.9-fold in PA28$\gamma^{-/-}$CoreTGvsWT). CK2 phosphorylates NS5A and regulates the production of infectious viral particles[87] and thus HCV pathogenesis (Table 2). CSNK2B was mapped to the enriched KEGG pathways "Adherens junction" ($p = 1.4 \times 10^{-13}$) and "Tight junction" ($p = 4.46 \times 10^{-7}$), some components of which are implicated in HCV entry and infection.[88]

SHC3 and TNR were decreased 1.9- and 4.62-fold, respectively, in PA28$\gamma^{-/-}$CoreTGvsCoreTG and were mapped to the enriched KEGG pathway "Focal adhesion" ($p = 3.56 \times 10^{-12}$; Table 1; Table S5), which regulates cell migration and adhesion to the extracellular matrix. Its deregulation is linked with tumor progression and possibly HCV propagation.[45] Previously, a Core interacting protein ENO1, associated with the focal adhesion, was identified as a novel regulator of HCV replication and release,[22] suggesting that SHC3 and TNR may play important roles in HCV pathogenesis.

Cell Growth and Death

Host cell apoptosis plays a critical role in HCV pathogenesis. The induction of apoptosis in the hepatocytes contributes to cell damage and fibrosis, whereas the induction of apoptosis in the peripheral blood mononuclear cells (PMBC), such as the T-cells, contributes significantly to the impaired immune response and HCV persistence in the host.[89−94] PA28γ is implicated in the cell cycle regulation, cell proliferation, and apoptosis[95−98] and likely plays a critical role in the manipulation of the cell cycle and apoptosis in HCV pathogenesis.

PPP3CA, TRADD, PRKAR2A, and IKBKG, with increased or decreased abundances in PA28$\gamma^{-/-}$CoreTGvsCoreTG, were mapped to KEGG pathway "Apoptosis" ($p = 1.84 \times 10^{-15}$; Table S5). PPP3CA was also mapped to "Oocyte meiosis" ($p = 9.84 \times 10^{-10}$; Table S5), associated with cell division. PPP3CA levels were highly elevated (12.94-fold) in PA28$\gamma^{-/-}$CoreTGvsCoreTG (Table 1), which may contribute to the accelerated cell death and the lack of tumor progression in PA28$\gamma^{-/-}$CoreTG mice.

PRKAR2A levels were decreased 1.88-fold in PA28$\gamma^{-/-}$CoreTGvsCoreTG (Table 1). PRKAR2A codes for a regulatory subunit of the cAMP dependent protein kinase (PKA), an important mediator of the cAMP signal transduction and elevated PRKAR2A expression is associated with an increased proliferation of the rat alveolar cells.[99] The suppression of PRKAR2A activity may therefore contribute to the lack of tumor proliferation in the PA28$\gamma^{-/-}$CoreTG mice.

Prioritization and Validation of the Novel Candidates for Their Role in HCV Replication and Release

Target prioritiszation using TargetMine is a simple process that involves uploading an initial list of candidates (in this instance the proteins in the CoreTGvsWT, PA28$\gamma^{-/-}$CoreTGvsWT, and PA28$\gamma^{-/-}$CoreTGvsCoreTG extended PPI networks) and estimating enriched biological themes associated with the input list.[16] Knowledge-based inputs may then be employed to further screen the proteins mapped to the top ranking significant associations to infer a manageable set of candidates. With the help of TargetMine, we previously investigated the significance of interactions between HCV Core and NS4B proteins and host factors in HCV infection and identified three novel regulators of HCV replication and propagation.[22]

dx.doi.org/10.1021/pr300121a | J. Proteome Res. 2012, 11, 3664−3679

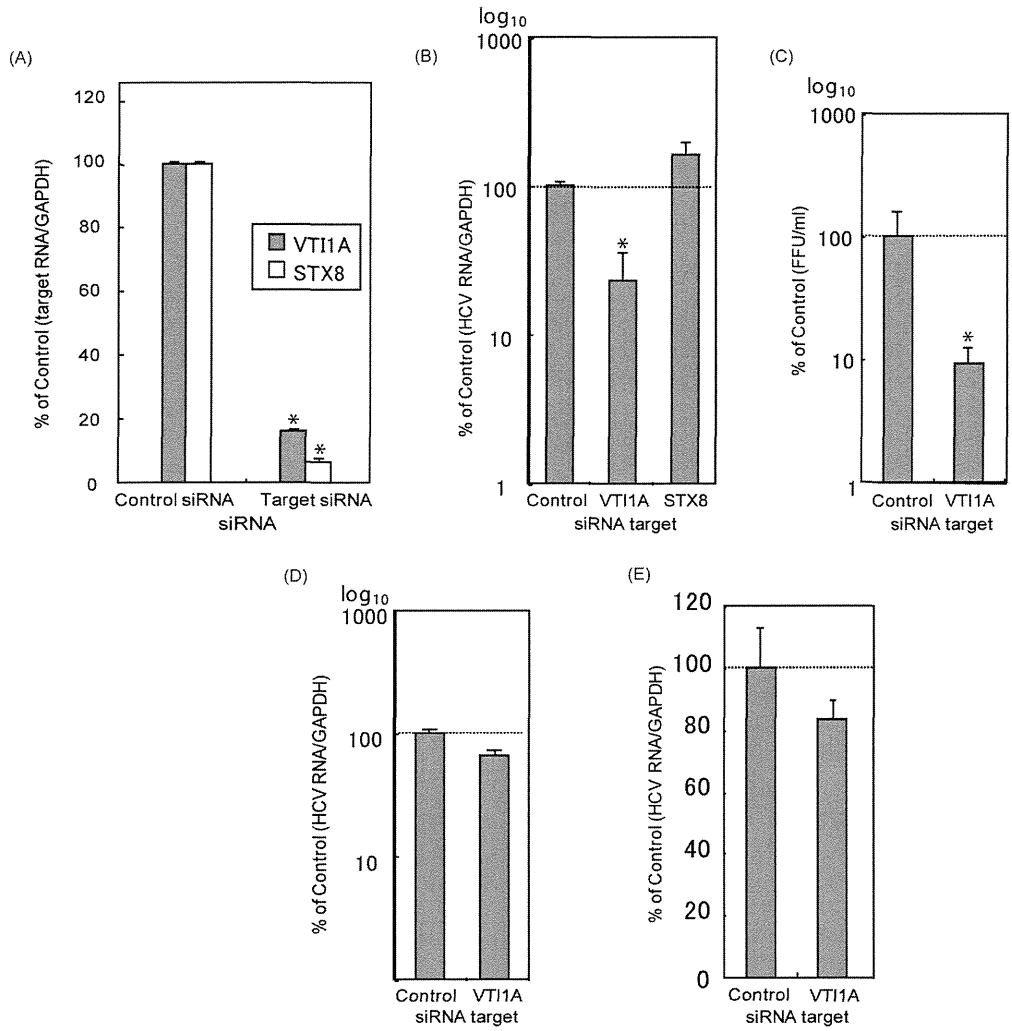

Figure 4. Effects of knockdown of candidate proteins on HCV propagation and replication. Host proteins VTI1A and STX8 were suppressed by RNAi (A) in Huh7OK1 cells infected with HCV JFH1 strain (genotype 2a; B, C, D) and in cells including subgenomic JFH1 replicon (E). The amounts of mRNA of the intracellular host proteins (A) and the supernatant viral RNA (B), viral titer (C), and intracellular viral RNA were estimated (D). The amount of the subgenomic viral RNA was also estimated (E). Each value was represented as percentage of the cells transfected with control siRNA; FFU: focus-forming units; * $p < 0.01$.

Table 3 summarizes the prioritized candidates and pathways, all of which have been discussed above. Traditionally, viral and host proteins associated with the HCV lifecycle (internalization, replication, assembly, and release) have been preferred targets in the anti-HCV studies. The prioritized candidates and pathways in Table 3a fall within this category. In particular, our analysis suggested novel and potentially crucial roles of the host proteins VTI1A and STX8, which were elevated in CoreTG but not in PA28$\gamma^{-/-}$CoreTG, in the replication and/or the release stages of the HCV lifecycle, therefore making these host proteins attractive targets for further investigation.

Because of the lack of a suitable model system for HCV infection, cell-culture-based systems for HCV RNA replication and infectious viral particle production have been extensively exploited to identify potential anti-HCV drug targets.[5,7−9] To further explore the roles of selected candidates in the HCV life cycle, we performed cellular assays to assess the impact of VTI1A and STX8 siRNA knockdowns on HCV replication and release. Since the HCV-production systems using the HCV JFH1 infectious strain (genotype 2a) isolates alone are capable of both efficient replication and the production of the infectious HCV particles,[33,100] JFH1 was used to infect the Huh7OK1 cell line 24 h after transfection with each siRNA (see Materials and Methods). The infected cells were harvested after 72 h post-infection and the expression of each host protein was assessed by qRT-PCR (Figure 4A). Supernatant viral RNA and the viral titer were significantly decreased by the knockdown of VTI1A but were unaffected by the STX8 knockdown (Figure 4B,C). However, VTI1A and STX8A knockdowns had no effect on the intracellular viral RNA levels in the HCV infected cells (Figure 4D) or replicon cells derived from JFH1 strain (Figure 4E) or replicon cells derived from the Con1 (genotype 1b) strain (data not shown). These observations suggest that VTI1A regulates HCV propagation but not HCV replication.

The standard therapy of PEGylated interferon-α plus rebavirin treatment often results in severe side effects such as depression, flu-like symptoms, anemia, and fatigue that force the treatment to discontinue in affected patients, thus necessitating improved and combinatorial treatment strategies.[101,102] The genetic variability of HCV has led to increasing drug resistance. Thus, antivirals that target host proteins critical to viral pathogenesis, with a lower rate of mutation and

dx.doi.org/10.1021/pr300121a | J. Proteome Res. 2012, 11, 3664−3679

preferably with minimal adverse side effects, may provide attractive alternatives to HCV protein targets. VTI1A-deficient (knockout) mice are viable and fertile,[55] suggesting that the suppression of VTI1A activity may not have significantly undesirable side effects.

Inhibition of COMT (which was increased 2.71- and 2.96-fold in CoreTGvsWT and PA28$\gamma^{-/-}$CoreTG, respectively; Table 1) activity via siRNA knockdown was previously shown to result in a decreased HCV replication in cells infected with the Con1 strain.[103] To investigate other possible aspects (such as genotype specificity) of COMT function in the HCV life cycle, we assessed the impact of the COMT siRNA knockdown on HCV replication and release. COMT knockdown, however, had no effect on HCV propagation or replication in the cells including full length or subgenomic replicons derived from JFH1 or Con1 strains (data not shown). The discrepancy between our observations and those of Chan et al.[103] may be explained by the differences in the methodologies. We employed a transient transfection method to knockdown the selected targets to assess their roles in HCV replication and release, whereas Chan et al. employed a lentiviral expressing system for their experiments. Lentiviral mediated siRNA delivery is known to result in a persistent knockdown of gene expression,[104] and a persistent knockdown of COMT expression may be necessary to inhibit HCV replication *in vitro*.

That we were able to experimentally validate one of the three genes selected for experimental characterization reinforces the strengths of the elaborate PPI network-based approach to identify and prioritize suitable targets for experimental and therapeutic investigation.

CONCLUSIONS

By analyzing high-throughput proteomics data from transgenic mice expressing HCV Core protein in the liver (an *in vivo* model of HCV pathogenesis) with or without the knockout of the proteasome activator PA28γ, we highlighted the cellular responses to HCV infection *in vivo* and obtained further insights into the role of PA28γ in HCV infection.

We investigated the network context of the changes in the protein abundances by mapping them onto the human interactome with the help of the TargetMine data warehouse. The differentially expressed proteins that were integrated with the human interactome were observed to participate in compact and well connected cellular networks reflecting the ability of HCV to rapidly and efficiently react to the host responses to HCV infection. A functional analysis of the PPI networks highlighted the cellular pathways associated with vesicular transport, immune system, cellular adhesion, cell growth, and cell death among others that were most prominently influenced by Core and PA28γ in HCV infection. We also confirmed the previous observations that host factors such as AKT1, BAX, CASP8 CDH1, COMT, MCM2, PTPN11, and RB1 showed increased or decreased abundances in HCV infection. However, to the best of our knowledge, the precise molecular mechanisms of these factors' involvement in HCV pathogenesis and HCC were unknown, and our analysis suggests novel contributions of Core and PA28γ to the functions of these proteins.

Our observations were then used to prioritize potential candidates for the follow-up experimental investigations. Cellular assays based on siRNA knockdowns of selected candidates in the HCV infected and replicon cells validated VTI1A, a SNARE protein associated with vesicular transport, which was upregulated in CoreTG but not in PA28$\gamma^{-/-}$CoreTG, as a novel regulator of HCV propagation but not replication. VTIA-deficient mice are largely indistinguishable from the normal mice except for minor growth retardation in a few instances; therefore, VTI1A is a promising novel candidate for anti-HCV therapy.

Our analysis not only builds on the present understanding of the Core-PA28γ interplay in HCV infection but also provides novel insights that would facilitate the clinical evaluation of proteomic changes associated with HCV pathogenesis. Our analysis also provides a generic framework for investigating large scale proteomic data. Such investigation may help identify common themes associated with different physiological conditions, especially pathogen (such as viral) infection and disease, and help develop effective broad spectrum strategies aimed at ameliorating pathogen infection and diseases.

ASSOCIATED CONTENT

Supporting Information

This material is available free of charge via the Internet at http://pubs.acs.org.

AUTHOR INFORMATION

Corresponding Author

*Tel: +81-72-641-9890. Fax: +81-72-641-9881. E-mail: kenji@nibio.go.jp.

Author Contributions

‖These authors contributed equally to this work.

Notes

The authors declare no competing financial interest.

ACKNOWLEDGMENTS

This study was supported by the Industrial Technology Research Grant Program in 2007 from New Energy and Industrial Technology Development Organization (NEDO) of Japan and also by grants-in-aid from the Ministry of Health, Labor, and Welfare; the Ministry of Education, Culture, Sports, Science, and Technology; the Osaka University Global Center of Excellence Program; and the Foundation for Biomedical Research and Innovation. We gratefully acknowledge Dr. T. Wakita for providing us with cell lines and plasmids.

REFERENCES

(1) Dubuisson, J. Hepatitis C virus proteins. *World J. Gastroenterol.* **2007**, *13* (17), 2406–15.

(2) Moriishi, K.; Mochizuki, R.; Moriya, K.; Miyamoto, H.; Mori, Y.; Abe, T.; Murata, S.; Tanaka, K.; Miyamura, T.; Suzuki, T.; Koike, K.; Matsuura, Y. Critical role of PA28gamma in hepatitis C virus-associated steatogenesis and hepatocarcinogenesis. *Proc. Natl. Acad. Sci. U.S.A.* **2007**, *104* (5), 1661–6.

(3) Myrmel, H.; Ulvestad, E.; Asjo, B. The hepatitis C virus enigma. *APMIS* **2009**, *117* (5–6), 427–39.

(4) Tang, H.; Grise, H. Cellular and molecular biology of HCV infection and hepatitis. *Clin. Sci. (London)* **2009**, *117* (2), 49–65.

(5) Moradpour, D.; Penin, F.; Rice, C. M. Replication of hepatitis C virus. *Nat. Rev. Microbiol.* **2007**, *5* (6), 453–63.

(6) Simmonds, P.; Bukh, J.; Combet, C.; Deleage, G.; Enomoto, N.; Feinstone, S.; Halfon, P.; Inchauspe, G.; Kuiken, C.; Maertens, G.; Mizokami, M.; Murphy, D. G.; Okamoto, H.; Pawlotsky, J. M.; Penin, F.; Sablon, E.; Shin, I. T.; Stuyver, L. J.; Thiel, H. J.; Viazov, S.; Weiner, A. J.; Widell, A. Consensus proposals for a unified system of nomenclature of hepatitis C virus genotypes. *Hepatology* **2005**, *42* (4), 962–73.